Batchelor, A.R. and Ferrari-John, R.S. and Katrib, Juliano and Udoudo, O.B. and Jones, D.A. and Dodds, Chris and Kingman, S.W. (2016) Pilot scale microwave sorting of porphyry copper ores: Part 1: laboratory investigations. Minerals Engineering, 98 . pp. 303-327. ISSN 0892-6875

Minerals Engineering 98 (2016) 303-327

Pilot scale microwave sorting of porphyry copper ores: Part 1 – Laboratory investigations

A.R. Batchelor *, R.S. Ferrari-John, J. Katrib, O. Udoudo, D.A. Jones, C. Dodds, S.W. Kingman

Faculty of Engineering, The University of Nottingham, University Park, Nottingham, NG7 2RD, United Kingdom

* Corresponding author. Tel.: +44 (0)115 951 4080; fax: +44 (0)115 951 4115. E-mail address: andrew.batchelor@nottingham.ac.uk (A.R. Batchelor)

Keywords

Microwave; Ore; Copper; Sorting; Infrared; Pilot Scale.

Highlights

- Microwave infrared thermal (MW–IRT) sorting of porphyry copper ores is investigated
- Microwave treatment energy dose drives ultimate average temperature rise
- Microwave treatment conditions have little effect on sortability performance
- Microwave-heating gangue minerals cause deviation from intrinsic sortability
- MW–IRT can effect separation of low value material for many porphyry copper ores

Abstract

Microwave treatment followed by infrared thermal imaging (MW–IRT) has been proposed as a potential excitation-discrimination technique to facilitate sorting of porphyry copper ores. A continuous, high throughput (up to 100t/h), belt–based microwave cavity operating at up to 100kW has been designed to interface directly with commercially available sorters at industrially relevant scales. In this paper, the fragment-by-fragment thermal response of 16 porphyry copper ore samples following microwave treatment in the bespoke system is evaluated to elucidate key performance criteria and identify likely candidate ores for microwave sorting. Microwave treatment energy dose was found to be the driving force behind the ultimate average temperature fragments experience, with other process variables (e.g. belt speed, power, belt mass loading, thermal equilibration time) having little effect on sortability performance. While fragment mineralogical texture and ore textural heterogeneity were shown to influence the average temperature rise of the fragment surface presented to the thermal camera, in most cases this variability did not adversely affect sortability performance. An abundance of microwave-heating gangue minerals (e.g. iron sulphides, iron oxides and hydrated clays) was shown to be the dominant source of deviation from intrinsic sortability. However, low average moisture content and co-mineralisation of copper and iron sulphides (or bulk sulphide sorting) was found to mitigate the deviation and provide better sortability performance. An attractive separation could be proposed for many of the ores tested, either to remove a large proportion of barren fragments from ore-grade material or concentrate a large proportion of copper values from waste-grade material.

http://dx.doi.org/10.1016/j.mineng.2016.07.007

1 Introduction

Recent advances in automated sorting technology has meant it has become widely cited as an emerging and potentially viable means to help address the challenges faced by sustainable hard rock mining, particularly in the forecasted low-grade and high energy demand future (Daniel and Lewis-Gray, 2011; Drinkwater et al., 2012; Lessard et al., 2014; Lessard et al., 2016; Napier-Munn, 2015; Pokrajcic et al., 2009; Powell and Bye, 2009). During the mining process, waste-grade or barren material may be introduced to run-of-mine (ROM) ore by planned and unplanned dilution of the ore reserve as well as internal dilution from poorly mineralised regions of the ore body. Processing such material through a conventional energy-intensive concentrator is very costly, due to both increased throughput and potential value losses to tailings. It is highly desirable to remove this unwanted material prior to beneficiation so that resources are not spent on treating the material for no return. Indeed, a recent study by Ballantyne and Powell (2014) showed ore grade was the greatest determinate of specific comminution energy when compared with other factors such as circuit efficiency, ore competency and grind size. In summary, scavenging high-grade material from waste/low-grade ore or pre-concentration by early rejection of barren gangue may offer the following benefits to a mining operation:

- Extend ore reserves and/or unlock previously uneconomic ore resources
- Increase metal production by raising the head grade to the concentrator
- Reduce metal specific processing and waste handling costs, and reduce water and energy consumption
- Increase mining rate for given mill capacity or reduce plant footprint
- Support alternative processing options, e.g. direct high-grade ore to crush-grind-float circuit and low-grade ore to heap leaching
- Remove deleterious minerals prior to downstream processing

Sorting of ores and other materials is typically performed in four to five stages, namely ore/particle preparation, presentation, excitation and/or discrimination, and separation. Figure 1 illustrates the unit processes involved with the relationship of material and data flows in the system.

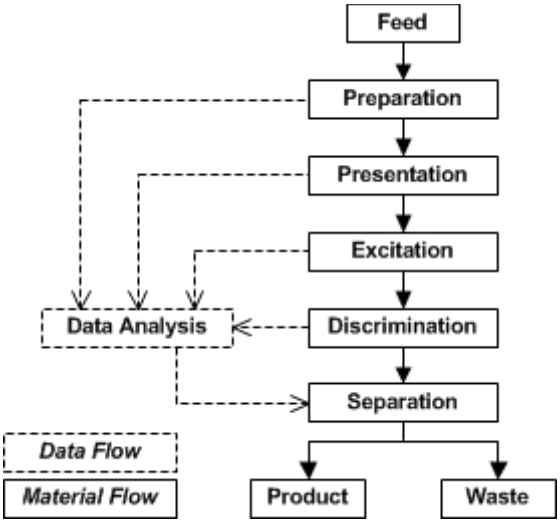

Figure 1: Operational processes in ore sorting

The excitation-discrimination step may be used to interrogate individual fragments or incremental lots of a bulk sample. The choice will be dependent on the methods used, the impact on throughput for the required feed presentation and the costs associated with the complexity of the separation system. Compressed air or water jet ejection systems are commonly employed for individual particle separation, whereas diverter gates/flaps are typically used for incremental lots on bulk streams.

There are many excitation-discrimination techniques used in industry to measure particular properties of materials, including nuclear (e.g. radiometric), optical (e.g. colour, fluorescence), electrical and magnetic (e.g. permittivity, permeability and conductivity), and thermal (e.g. emissivity). These techniques utilise a wide range of the electromagnetic spectrum, including gamma rays and x-rays, ultraviolet, visible and infrared light, microwaves and radiowaves (Adair et al., 2013; Knapp et al., 2014; Murphy et al., 2012; Salter and Wyatt, 1991; Seerane and Rech, 2011), illustrated in Figure 2. Whilst a number of techniques are available and have been demonstrated at industrially relevant scales for commodities such as diamonds and industrial minerals (Riedel and Dehler, 2010; Sivamohan and Forssberg, 1991), none have been proven to give the required discrimination and support the high throughputs required for low-grade finely disseminated porphyry copper ores. Porphyry copper ores are particularly important because they currently account for around 50-60% of global copper production as well as being significant sources of gold, silver, molybdenum and other by-product metals (BGS, 2007).

http://dx.doi.org/10.1016/j.mineng.2016.07.007

Electromagnetic Spectrum	Wavelength (m)	Sensor Type / Technology	Material Property Detected	Application
Gamma Radiation	10^{-12}	RM (Radiometric)	Natural Gamma Radiation	Fuel, Precious Metals
	10^{-11}			
	10^{-10}	X-ray Transmission (XRT)	Atomic Density	Base Metals, Precious Metals, Industrial Minerals, Diamonds, Fuel
X-rays	10^{-9}	X-ray Fluorescence (XRF)	Visible Fluorescence, X-rays Fluorescence	
	10^{-8}			
Ultraviolet (UV)	10^{-7}	COL (CCD Colour Camera)	Reflection, Absorption, Transmission, Shape	Base Metals, Precious Metals, Industrial Minerals, Diamonds
Visible Light	10^{-6}			
Near-Infrared (NIR)	10^{-5}	Photometric (PM)	Monochromatic Reflection/Absorption	
	10^{-4}	Near-Infrared Spectroscopy (NIR)	Reflection/Absorption	Base Metals, Industrial Minerals
Infrared (IR)	10^{-3}	Infrared Camera (IR)	Heat Conductivity / Dissipation	
Microwaves	10^{-2}	Microwave Attenuation		
	10^{-1}	**Microwave Heating with Infrared Thermal Imaging (MW–IRT)**	**Selective Heating (Metals Heat Faster than Other Minerals)**	**Base Metals (Proposed Application)**
	10^{0}			
Radiowaves	10^{1}	Radiofrequency (RF) Heating		
	10^{2}			
Alternating Current (AC)	10^{3}	Electro-Magnetic Sensor (EM)	Conductivity, Permeability	Base Metals
	10^{4}			

Figure 2: Sensing systems for sorters in the mining industry

Microwave heating has been proposed as a technique to selectively raise the temperature of ore fragments containing valuable minerals, providing a means of distinguishing fragments with different grades (Dimitrakis et al., 2014; Dormenval et al., 2014; Harding and Wellwood, 2010). The efficacy of this mechanism depends on rapid, volumetric and selective heating of certain mineral phases within the ore matrix. In particular, highly microwave-absorbent minerals (such as nickel, copper, iron and lead sulphides, magnetite and other minerals with bound and/or free water (e.g. smectite clay)) heat far more readily than common microwave-transparent rock-forming minerals (such as quartz, feldspars, micas and many other non-sulphide gangue minerals) (Chen et al., 1984; Chunpeng et al., 1990; Church et al., 1988; Harrison, 1997; Kingman et al., 2000; Kobusheshe, 2010; McGill and Walkiewicz, 1987; McGill et al., 1988; Nelson et al., 1989; Standish and Worner, 1991; Walkiewicz et al., 1988; Yixin and Chunpeng, 1996). Infrared thermal imaging may then be employed as a means of measuring differences in the thermal response of ore fragments to provide a basis for separation using conventional sorting technologies. Microwave heating offers a particular benefit for sorting applications in that the excitation step may be performed on bulk material, with the following discrimination and separation steps performed on individual fragments if desired. Decoupling the processing steps in this way allows for flexibility in designing microwave cavities to achieve high throughputs, thereby reducing microwave system requirements, overall plant complexity and total microwave energy consumption.

Investigations combining microwave heating with infrared thermal imaging (MW–IRT) have been carried out since the 1980s by a number of authors on lead-zinc sulphide, gold, copper sulphide, molybdenum sulphide and iron ores (Berglund and Forssberg, 1980; Ghosh et al., 2013; Ghosh et al., 2014; John et al., 2015; Jokovic et al., 2014; Rizmanoski and Jokovic, 2016; Sivamohan and Forssberg, 1991; Van Weert and Kondos, 2007; Van Weert et al., 2009; Wotruba and Scharrenbach, 2007). The authors reported varying degrees of sortability performance related to the mineralogy of the samples and the distribution of valuable minerals throughout the individual fragments analysed, demonstrating the applicability of microwave treatment to sorting applications. The experiments were typically conducted on small batches of material in low power (<3kW) 2.45GHz multimode cavities, such as those used in domestic kitchen microwave ovens. The treatment times were typically 10 seconds or greater, as this was the time taken for one or more full revolutions of the turntable, used to achieve the most homogeneous treatment possible in these cavities. As such, the microwave energies used were uneconomical (typically >>1kWh/t) and the residence times much longer than that required to achieve industrially relevant throughputs (typically requiring >100t/h).

A bespoke, high throughput and continuous pilot scale microwave sorting system capable of treating up to 100t/h of ore has been developed by The University of Nottingham and Rio Tinto Technology and Innovation. A laboratory microwave treatment system is based at the Nottingham campus and a full scale pilot plant with an incorporated industrial sorter situated at a major porphyry copper mine owned and operated by the project sponsor. The investigations detailed in the first part of this paper evaluate the fragment-by-fragment thermal response of 16

http://dx.doi.org/10.1016/j.mineng.2016.07.007

porphyry copper ore samples following microwave treatment in the laboratory based system. The specific objectives were to:

- Determine the influence of process conditions likely to be encountered in the industrial pilot plant on the thermal response and sortability of a variety of porphyry copper ores
- Determine the influence of gangue mineralogy on sorting performance
- Elucidate key performance criteria to identify likely candidate ores for high value microwave sorting
- Develop a method for the laboratory based system to provide an operating window for the industrial pilot plant

2 Materials and methods

2.1 Ore characterisation, particle size requirements and sample preparation

The porphyry copper ore samples used throughout this investigation were sourced from two host mines. Eight ore types were selected from each mine that covered a range of different lithologies with varying copper sulphide grade, copper sulphide to iron sulphide ratio and non-sulphide gangue mineralogy. The ores were supplied in three narrow size classes, namely -76.2+50.8mm, -50.8+25.4mm and -25.4+12.7mm, listed in Table 1.

Table 1

Sample list and number of fragments tested/analysed

Sample ID	Sample Grade *	-76.2+50.8mm	-50.8+25.4mm	-25.4+12.7mm
Mine 1				
1	Ore	-	200/100	-
2	Ore	-	200/100	-
3	Ore	-	200/100	-
4	Ore	-	200/100	-
5	Ore	-	200/100	-
6	Ore	-	200/100	-
7	Ore	-	200/100	-
8W	Waste	-	200/100	-
Mine 2				
9	Ore	100/50	100/50	150/150
9W	Waste	50/50	50/50	50/50
10	Ore	100/100	100/100	100/100
10W	Waste	100/50	100/50	100/50
11	Ore	100/50	100/50	100/50
11W	Waste	140/140	150/150	150/150
12	Pebbles	-	50/50	-
13	Pebbles	-	50/50	-

* Sample defined as “ore-grade” or “waste-grade” by host mine.

The three size classes were investigated separately to determine sortability within a narrow size range and to compare the different sizes, as well as to cover practical maximum and minimum particle sizes likely to be processed industrially. The particle top size is limited by the ability of the separation process (e.g. compressed air ejection) to efficiently alter the trajectory of heavy fragments. The particle bottom size is limited by the computational power required to analyse, and the ability to efficiently separate, the high fragment count rates encountered with small particles. These operational challenges also ultimately limit the throughput that can be achieved for a given size class through industrial sorters (Pascoe et al., 2010; Udoudo, 2010). The combined size range of -76.2+12.7mm has a top size to bottom size ratio of 6:1, which is also similar to a ratio of 4:1 that is typically considered the range for optimum performance of industrial sorting equipment. Widening the size range during testing allowed for some flexibility in determining the potential size range to be considered for an industrial application, especially if a larger range (e.g. 5:1) could be utilised. Finally, it has been demonstrated in many instances that sulphides tend to pre-concentrate in -12.7mm size fractions through selective breakage after early

http://dx.doi.org/10.1016/j.mineng.2016.07.007

comminution stages, raising the grade such that these sizes would not likely be targeted for sorting (Bamber, 2008).

Mine 1 provided seven ore-grade and one waste-grade (denoted with the suffix "W") ore for consideration, covering four broad lithology groups. Mine 2 provided an ore-grade and waste-grade version of three lithologies (quartzite, quartz-monzonite and limestone-skarn) plus two recycled pebbles samples. Although sorting a pebbles stream would not reap the full benefits associated with sorting ROM ore, it's relatively easy accessibility, reduced throughput requirement and effect on SAG milling performance make it an attractive location for trialling sorting technology with reduced risk (Lessard et al., 2016). Indicative modal mineralogies for the -50.8+25.4mm size samples were estimated by using a Mineral Liberation Analyser (MLA) (FEI, 2016) to measure polished sections of 20 representatively split lump fragments, given in Table 2 and Table 3. Samples #12 and #13 were not analysed using MLA. The dominant copper sulphide mineral in all samples was chalcopyrite. The dominant sulphide gangue was pyrite and other microwave-heating gangue included montmorillonite and iron oxides. The dominant non-sulphide and microwave-transparent gangue minerals were quartz, feldspar and mica. Several ores also had significant proportions of pyroxenes, amphiboles, garnets and carbonates.

The head assays for each of the 16 samples are presented in Table S.1 in the Supplementary Information. Any fragments that contained <0.1%Cu were considered to be effectively barren and uneconomic to process according to the project sponsors, and were then necessarily the main target for rejection. Processing economics further dictated that fragments between 0.1 and 0.25%Cu were of marginal grade or mineralised waste. The higher grade fragments were arbitrarily divided into 0.25–0.5%Cu, 0.5–1%Cu and >1%Cu by the authors to see the mass and copper distributions across different fragment grade classes, given in Table S.2 in the Supplementary Information.

Approximately 200–500kg of each ore was supplied and subsequently riffle split to produce between 50 and 200 representative fragments to be used as the test sample. The test fragments were washed to remove surface contamination, dried in an oven at low temperature (50°C), photographed to record surface features and numbered for identification. After microwave treatments were performed, each fragment was crushed and pulverised, and a representative subsample submitted for assay by X-ray fluorescence (XRF) to determine copper, iron and sulphur content.

Initial moisture content determination testing on analytical grade montmorillonite in a thermogravimetric analyser (TGA) suggested that the derivative mass loss (change in mass / change in temperature) reached a minimum at approximately 120°C. Moisture analyses on samples #9W, #12 and #13 from Mine 2 were carried out by TGA with a 10-20mg sample heated at 20°C/min to 120°C and held for 5 minutes. For samples #10 and #10W from Mine 2, a one gram sample was placed in an oven overnight at 120°C. The TGA experiments indicated that the mass loss at 120°C was approximately 15-20% higher than at 105°C. However, XRF analysis on selected samples indicated that there was no discernible change in sulphur content between heating at 105°C or 120°C, as it was within the measurement error from repeatability of testing. Furthermore, there was no observed correlation between higher mass loss and higher sulphur content for the fragments tested. Therefore, any potential oxidation of sulphides at the slightly elevated temperature was considered to be negligible. Moisture content was subsequently determined by the standard method of measuring the mass loss when heated to 105°C overnight in an oven for samples #1-8 from Mine 1 and samples #9, #11 and #11W from Mine 2.

At the beginning of the project, 50 fragments were considered for Mine 2 as initial scoping tests. The sample size was increased to 100 fragments and then to 150 fragments to improve representivity and data quality in an effort to account for the different heating responses encountered in ores with more heterogeneous textures. For many of the samples from Mine 2 and all of the samples from Mine 1, a larger initial test sample was taken and subjected to microwave treatment, after which every second fragment on an average temperature rise basis was selected for assay and further analysis. The justification for this procedure is described in detail in section 4.5.

http://dx.doi.org/10.1016/j.mineng.2016.07.007

Table 2

Modal mineralogy from Mine 1

Mineral	Modal Mineralogy (wt%)							
	Sample 1	Sample 2	Sample 3	Sample 4	Sample 5	Sample 6	Sample 7	Sample 8W
Microwave-heating phases								
Chalcopyrite	1.9	5.9	2.8	1.5	2.3	4.7	2.0	0.2
Other Copper Sulphides [a]	<0.1	0.1	0.3	<0.1	<0.1	<0.1	<0.1	0.0
Pyrite [b]	2.5	2.8	3.2	0.8	1.7	2.9	3.3	2.0
Montmorillonite	0.8	0.4	1.5	0.6	0.8	1.9	2.1	1.4
Iron Oxides [c]	1.4	0.7	1.4	1.5	2.3	0.7	0.6	5.0
Microwave-transparent phases								
Quartz	33.1	39.1	39.2	27.7	22.8	40.0	28.9	21.6
Feldspar [d]	30.3	21.8	15.5	43.3	42.3	19.7	38.3	32.7
Muscovite	23.9	26.9	29.6	17.6	19.4	25.3	19.9	14.1
Other Micas [e]	5.0	1.3	3.5	5.5	7.2	3.1	4.3	18.7
Pyroxene/Amphibole	<0.1	<0.1	0.1	0.1	0.1	<0.1	<0.1	2.1
Carbonates/Sulphates [f]	0.5	0.3	2.4	0.8	0.7	1.1	0.1	0.5
Other	0.6	0.8	0.6	0.7	0.7	0.7	0.5	1.7

[a] Other Copper Sulphides included bornite, chalcocite, tennantite and covellite.
[b] Pyrite includes other trace sulphides such as pyrrhotite, molybdenite, galena and sphalerite.
[c] Iron Oxides included magnetite, hematite, ilmenite and other Fe-Ti oxides.
[d] Feldspars included orthoclase, plagioclase and albite.
[e] Other Micas included biotite, phlogopite and chlorite-group minerals.
[f] Carbonates/Sulphates included calcite, dolomite and gypsum.

Table 3

Modal mineralogy from Mine 2

Mineral	Modal Mineralogy (wt%)					
	Sample 9	Sample 9W	Sample 10	Sample 10W	Sample 11	Sample 11W
Microwave-heating phases						
Chalcopyrite	1.1	0.8	1.0	0.1	0.8	0.2
Other Copper Sulphides [a]	<0.1	<0.1	0.5	0.2	<0.1	0.0
Pyrite [b]	4.3	2.5	0.7	2.6	8.3	3.3
Montmorillonite	2.2	0.6	0.3	0.4	0.9	0.3
Iron Oxides [c]	0.3	0.5	0.2	<0.1	1.1	0.1
Microwave-transparent phases						
Quartz	36.8	24.3	89.5	88.5	20.2	36.0
Feldspar [d]	31.5	47.8	2.2	1.5	20.4	28.3
Biotite/Phlogopite	16.4	18.0	4.1	4.7	1.2	10.4
Other Micas [e]	3.3	3.6	1.2	1.8	1.3	2.3
Pyroxene/Amphibole	1.4	0.7	0.1	0.1	20.7	16.3
Carbonates/Sulphates [f]	0.3	0.2	0.0	0.0	4.7	1.5
Garnets	0.4	0.0	0.0	0.1	13.7	0.2
Other	2.0	1.0	0.3	0.1	6.7	1.1

[a] Other Copper Sulphides included bornite, chalcocite, tennantite and covellite.
[b] Pyrite includes other trace sulphides such as pyrrhotite, molybdenite, galena and sphalerite.
[c] Iron Oxides included magnetite, hematite, ilmenite and other Fe-Ti oxides.
[d] Feldspars included orthoclase, plagioclase and albite.
[e] Other Micas included muscovite and chlorite-group minerals.
[f] Carbonates/Sulphates included calcite, dolomite and gypsum.

http://dx.doi.org/10.1016/j.mineng.2016.07.007

2.2 Microwave treatment system

The continuous pilot scale microwave treatment system was comprised of a bespoke pentagonal cavity with integrated reflective and resistive chokes (Kingman et al., 2013), fed by a 10-100kW variable power e2v generator operating at 896MHz. The generator was connected by rectangular WR975 waveguide to a three stub automatic impedance matching device (or tuner) prior to the applicator.

The applicator was designed to heat a shallow layer (e.g. monolayer) of fragments covering 76.2–12.7mm in size (nominally 50.8mm) arranged on a flat, horizontal and thin microwave-transparent silicone conveyor belt by providing an electric field pattern that resulted in a homogenous cumulative energy across the belt (to within approximately ±20%) when summed along the direction of travel. Providing a homogeneous treatment of the ore is critical to the excitation process as it allows the fragment thermal response to be based on their individual mineralogy and not influenced by position in the cavity. The speed of the conveyor belt and ore loading could be adjusted to achieve throughputs of approximately 10-100t/h, resulting in a microwave treatment energy dose range of 0.1-10kWh/t. The design of the applicator is described in detail by Katrib et al. (2016).

The horizontal belt arrangement was specifically chosen for this pilot scale system to allow for a direct and simple interface with a horizontal belt industrial sorter when operating continuously. However, in these investigations the system was operated in batch to assess the test fragments without use of a sorter to effect separations. Figure 3 illustrates the batch microwave treatment sequence used to ensure that the test fragments were treated under steady-state conditions. Sacrificial ore of the same material as the test sample was loaded onto the belt either side of the test fragments. The test fragments were initially positioned outside of the cavity while the microwave power was turned on and ramped up to the set power level, typically only taking one or two seconds. The choking structures either side of the cavity were designed to confine the vast majority of the electric field within the cavity; therefore, the test fragments received negligible microwave energy during the brief ramp cycle when outside the cavity. Once power was at the set level, the conveyor belt was started and the test fragments treated at the chosen conditions. Once the test fragments had exited the cavity, microwave power was switched off. The material was then run out of the applicator until the test fragments were positioned within the field of view of the NEC H2640 thermal imaging camera used in these investigations, which was mounted above the conveyor belt.

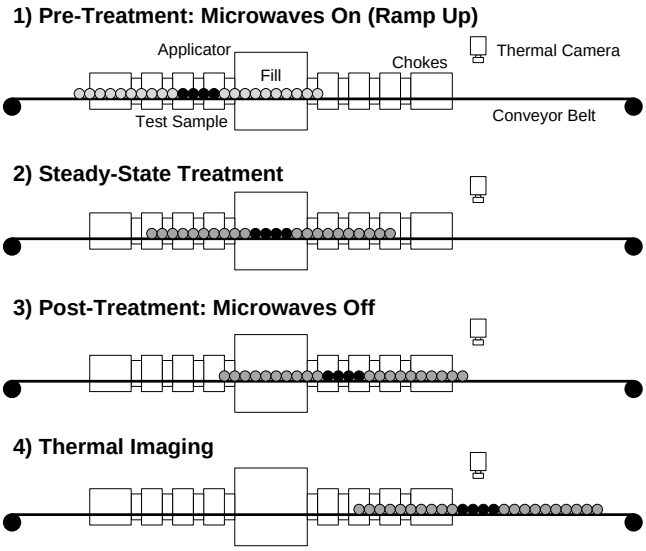

Figure 3: Microwave treatment procedure

A variety of process conditions were tested as part of these investigations and given in Table 4. The belt mass loading was ore dependent due to differing fragment sizes and shapes within each size class, but was also controlled at 100% (monolayer) and approximately 60% (spaced monolayer) belt area coverage to mimic the coverage required for discrimination on an industrial sorter. The belt speed was adjusted between 0.3 and 1m/s and incident (forward) microwave power adjusted between 10 and 55kW to achieve throughputs between 15 and 80t/h at microwave treatment energy doses of 0.3–1kWh/t.

http://dx.doi.org/10.1016/j.mineng.2016.07.007

Table 4

Microwave treatment condition ranges

Parameter	Units	Size Class		
		-76.2 +50.8mm	-50.8 +25.4mm	-25.4 +12.7mm
Mass Loading	kg/m	14-40	7-27	9-12
Belt Speed	m/s	0.3-0.7	0.3-1.0	0.4-1.0
Throughput	t/h	25-80	15-80	15-30
Forward Power	kW	10-55	10-55	10-25
Dose	kWh/t	0.3-1.0	0.4-1.0	0.4-1.0

2.3 Fragment presentation

Fragment presentation is an important consideration for efficient separation in sorters, but it is also important when interrogating the thermal response of ore fragments. John et al. (2015) and Rizmanoski and Jokovic (2016) conducted MW–IRT trials on synthetic ore particles to determine the effects of microwave-absorbent mineral dissemination on the surface thermal response observed. It was elucidated that the coarser the microwave-absorbent grains (and/or the greater the degree of clustering of finer grains) and the closer to the surface they occur, the higher the surface temperature measurement recorded for a given equilibration time after treatment. These observations indicated that coarser fragments (such as the -76.2+50.8mm size class) may be more susceptible to variations in surface temperature measurement than finer fragments (such as the -25.4+12.7mm size class) if the microwave-absorbent minerals are not distributed evenly throughout the individual fragments. Furthermore, by evaluating separate narrow size fractions the load topography and mass distributions were kept more even as there was not a large variety in particle size across and along the belt.

To address these challenges, it was decided to conduct experiments on the test fragments in two orientations in order to inspect the majority of the fragment surface after microwave treatment. In practice, it is possible for industrial sorters to measure the entire fragment surface at the same time by having multiple sensors look at particles from different directions. The first orientation, Orientation 1 (O1), was chosen as the “most stable” orientation where the fragment rested on its flattest surface. The fragment was then flipped upside down to reveal the opposite surface for Orientation 2 (O2) and microwave treatments conducted under the same conditions as for Orientation 1.

2.4 Thermal image analysis

The test fragments and sacrificial ore were arrayed on the conveyor belt in the chosen mass loading conditions. The fragments were allowed to equilibrate to room temperature prior to every test to ensure there was negligible variation in the starting temperature of each fragment that might adversely affect temperature rise comparisons. A pre-treatment, or “cold”, thermal image of the test fragments was captured. The microwave treatment sequence was executed and post-treatment, or “hot”, thermal images were recorded at one frame per second for two minutes. Figure 4 gives an example of the images captured for the test fragments. The hot images were recorded for up to two minutes in order to understand the evolution of thermal profiles over a prolonged period that would cover the transition from the microwave treatment system to a sorter on a hypothetical continuous industrial system. Depending on the belt speed used, the time to the first recorded hot thermal image was in the order of 10-30 seconds.

RC Radiometric Complete Online (GORATEC Thermography Studio) thermal imaging software was used to extract data from the thermal images. Each fragment pre- and post-microwave treatment was carefully and manually traced by a custom polygon to delineate the boundary between touching fragments and conveyor belt in the background. The software then extracted the average, minimum and maximum temperatures for each polygon, as well as a histogram of temperatures measured for each polygon and each frame recorded over the two minutes. The change in temperature of the fragments due to microwave treatment was typically described as Average Temperature Rise (ΔT_{ave}); that is, the average temperature of the fragment post-microwave treatment minus the average temperature pre-microwave treatment.

http://dx.doi.org/10.1016/j.mineng.2016.07.007

[a] 

[b] 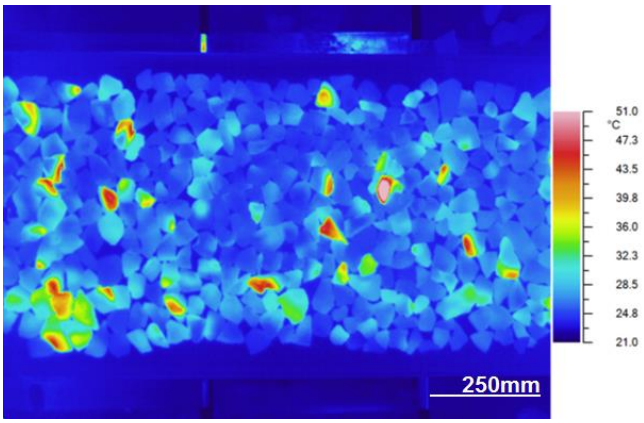

Figure 4: Example [a] test fragment layout and [b] thermal image after microwave treatment for -50.8+25.4mm fragments

2.5 Calculating ore sortability performance

Sortability performance was determined by comparing the intrinsic sortability of the ore to the actual sortability of the ore using the MW–IRT technique. Intrinsic sortability is the best possible separation that may be achieved and is dependent on the distribution of the valuable minerals across the ore fragments. By ranking fragments from the highest to the lowest grade and cumulating grade, mass recovery and values recovery, grade-recovery curves may be constructed and sortability calculated at given mass rejections. Actual MW–IRT sortability is then defined by ranking the fragments from the highest to lowest ΔT_{ave}, presuming that the minerals of interest are microwave-absorbent such that a higher ΔT_{ave} corresponds to a higher grade. The closer the two grade-recovery curves are to each other, the better the sorting performance obtained. The sortability performance for a given mass of product, or accepts, may be calculated according to Eq. (1), which was developed by Tucker et al. (2013):

$$P_{xx} = ((A_{XX} - 1)/(I_{XX} - 1)) \times 100\% \quad (1)$$

where, P_{XX} is the sortability performance index (i.e. performance of the actual excitation/detection system against the potential of the intrinsic sortability), I_{XX} is the intrinsic grade concentration factor (defined as the grade of the richest xx% by mass divided by the feed grade), and A_{XX} is the actual grade concentration factor (defined as the grade of the hottest xx% by mass divided by the feed grade). When scavenging values from waste-grade ore it would be typical to consider the richest 0-50% of the ore by mass (e.g. A_{25}, I_{25} and P_{25}), whereas for rejection of barren gangue from ore-grade material it would be typical to consider the richest 50-100% of the ore by mass (e.g. A_{75}, I_{75} and P_{75}).

According to these definitions, a sortability performance index of zero means that MW–IRT sorting is acting as a random splitter and a negative sortability performance index means that the colder fragments have a higher grade; essentially reverse sorting according to the presumption that a higher ΔT_{ave} corresponds to a higher grade. Reverse sorting is mineralogically possible if low grade fragments contain a high proportion of other microwave-absorbent gangue whereas high grade fragments do not, such that it results in a higher temperature rise for the low grade fragments.

3 The influence of process conditions on fragment thermal response

3.1 Microwave treatment repeatability

Several test conditions were run in duplicate for sample #13 to evaluate the repeatability of average temperature rise from the same microwave-treatments. Figure 5 gives the average ΔT_{ave} from duplicate testing with range bars for three different test conditions. The average absolute difference between the duplicate tests was approximately 0.3°C. The average standard deviation was 0.2°C, which equated to an average relative standard deviation of approximately 13%. It is worth noting that higher relative standard deviations were typically observed on lower ΔT_{ave} fragments, where a change of ±0.1–0.2°C constituted a high proportion of ΔT_{ave}.

http://dx.doi.org/10.1016/j.mineng.2016.07.007

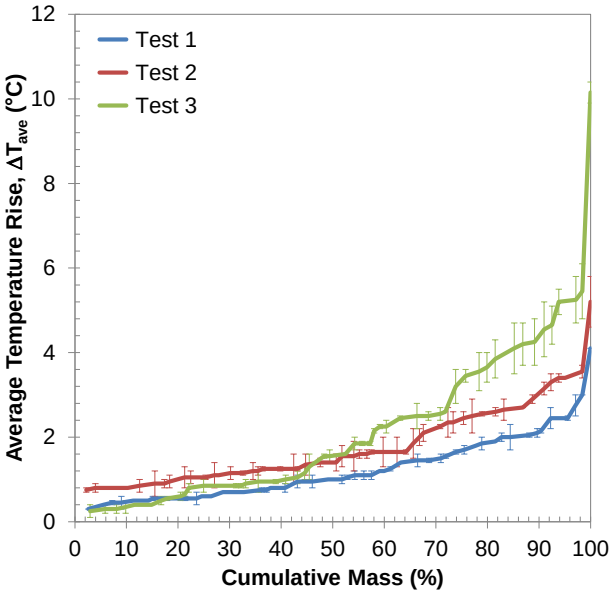

Figure 5: Average temperature rise repeatability for selected tests of sample #13

3.2 Belt loading, belt speed, microwave power and microwave dose

Increasing the belt loading from a 60% spaced monolayer to a 100% coverage monolayer arrangement had no singly discernable effect on the thermal profiles of the ore due to the fact that, to achieve the same dose, different belt speeds and powers were required for each scenario. Increasing the belt loading does allow for a greater throughput in the microwave system thereby utilising more of the system capacity; however, the belt loading can be subsequently reduced during the transition from the microwave to sorter systems by accelerating the particles to higher speeds for separation.

Comparing treatments for 100% coverage monolayers at equivalent dose but with different power and belt speeds sometimes yielded a slightly higher average temperature rise for higher power/speed combinations and with a greater selectivity between hot and cold fragments. However, in many instances the difference was negligible, within repeatability error or otherwise within a range expected by slight differences in microwave dose or thermal equilibration times. Figure 6 illustrates these thermal responses for sample #12 and -50.8+25.4mm size at three doses with two power/speed combinations. The thermal equilibration time for the temperature measurements was taken at approximately 10 seconds, which was the equilibration time taken to the first thermal image at 0.75m/s.

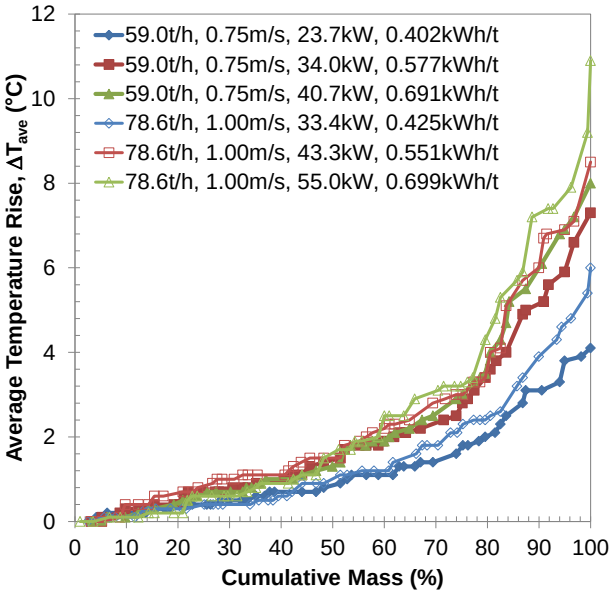

Figure 6: Sample #12 fragment thermal response profile due to belt speed, microwave power and microwave dose at -50.8+25.4mm size

http://dx.doi.org/10.1016/j.mineng.2016.07.007

Nevertheless, it can clearly be seen that microwave dose is the most important factor driving the average temperature rise and selectivity between hot and cold fragments; the higher the dose, the higher the ultimate average temperature rise, particularly for the hot fragments. Increasing the dose had little impact on the cold fragment temperature rise, which contained lesser amounts of microwave-absorbent material.

3.3 Fragment orientation

The effect of fragment orientation and fragment size on average temperature rise under equivalent microwave treatment conditions is illustrated for sample #9 in Figure 7 and summarised for samples #9-13 in Table 5. All treatments were performed at approximately 0.75kWh/t, with -76.2+50.8mm, -50.8+25.4mm and -25.4+12.7mm size fragments, and with thermal equilibration times of ranging from 10-30 seconds (depending on the belt speed for the particular sample under test). It can be seen that as the fragment size decreases, the variability in average temperature rise also decreases, particularly for the hotter fragments. This is due to the microwave-absorbent minerals occurring closer to both surfaces of the fragment at smaller sizes allowing for the heat to spread more evenly throughout each fragment shortly after microwave treatment.

The coefficient of determination (R^2) value for the observed data compared to the line of unity may be used as a measure of the thermal response variability. Importantly, in the vast majority of cases the difference in measured average temperature rise between orientations did not appear to make a hot fragment appear cold or vice versa, which might adversely affect sortability performance calculations when considering just one orientation. However, some fragments in some ores did exhibit large differences in average temperature rise between orientations due to coarse microwave-heating phase mineralisation and preferential clustering of microwave-heating phases on one side of the fragments under test.

The effect of fragment orientation and thermal equilibration time on average temperature rise under equivalent microwave treatment conditions is illustrated for sample #1 in Figure 8 and summarised for samples #1-8 in Table 6. All treatments were performed at approximately 1kWh/t, with -50.8+25.4mm size fragments and with thermal equilibration times of 20, 60 and 120 seconds. It can be seen that as thermal equilibration time increases, the variability in average temperature rise decreases. This is due to there being sufficient time for heat to spread more evenly throughout the fragments and for the maximum temperature, which can highly influence average temperature if there are hot spots on the surface of the fragment due to near-surface mineralisation, to also reduce.

In summary, the highest variation between orientations would be expected with coarser particles at shorter thermal equilibration times, and the lowest variation with finer particles at longer thermal equilibration times. It may therefore be expected that fragment orientation could play a role in sortability performance, particularly when looking to separate the hottest 0–50% (scavenging mode mentioned previously) from coarser fragment sizes shortly following microwave treatment.

Table 5

Fragment thermal response R^2 values for different orientations and sizes at ~0.75kWh/t

Sample	Size Class		
	-76.2+50.8mm	-50.8+25.4mm	-25.4+12.7mm
#9	0.2647	0.8240	0.9382
#9W	0.7327	0.7982	0.7235
#10	0.9065	0.6287	0.9654
#10W	0.7192	0.9310	0.8588
#11	0.6272	0.7766	0.9391
#11W	0.6568	0.5050	0.8791
#12	-	0.8869	-
#13	-	0.7665	-

http://dx.doi.org/10.1016/j.mineng.2016.07.007

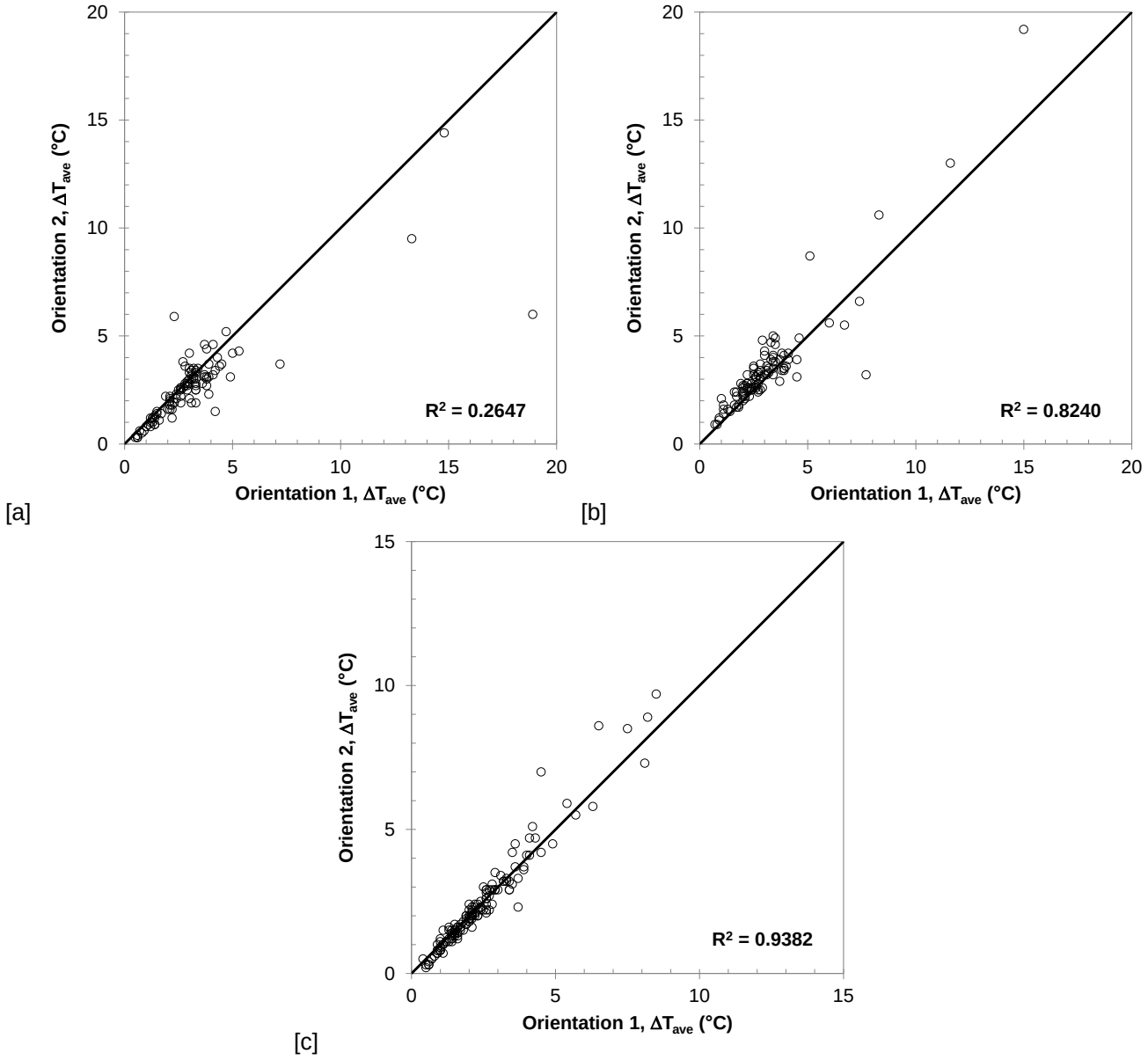

Figure 7: Sample #9 fragment thermal response for different orientations at [a] -76.2+50.8mm, [b] -50.8+25.4mm and [c] -25.4+12.7mm size and ~0.75kWh/t

Table 6

Fragment thermal response R^2 values for different orientations and thermal equilibrium times at ~1kWh/t

Sample	Thermal Equilibration Time		
	20s	60s	120s
#1	0.7143	0.8431	0.8762
#2	0.6942	0.7191	0.7475
#3	0.4602	0.7719	0.8569
#4	0.6960	0.8790	0.9138
#5	0.7319	0.8446	0.8768
#6	0.8441	0.8713	0.9246
#7	0.6984	0.8389	0.8719
#8W	0.7000	0.7861	0.8164

http://dx.doi.org/10.1016/j.mineng.2016.07.007

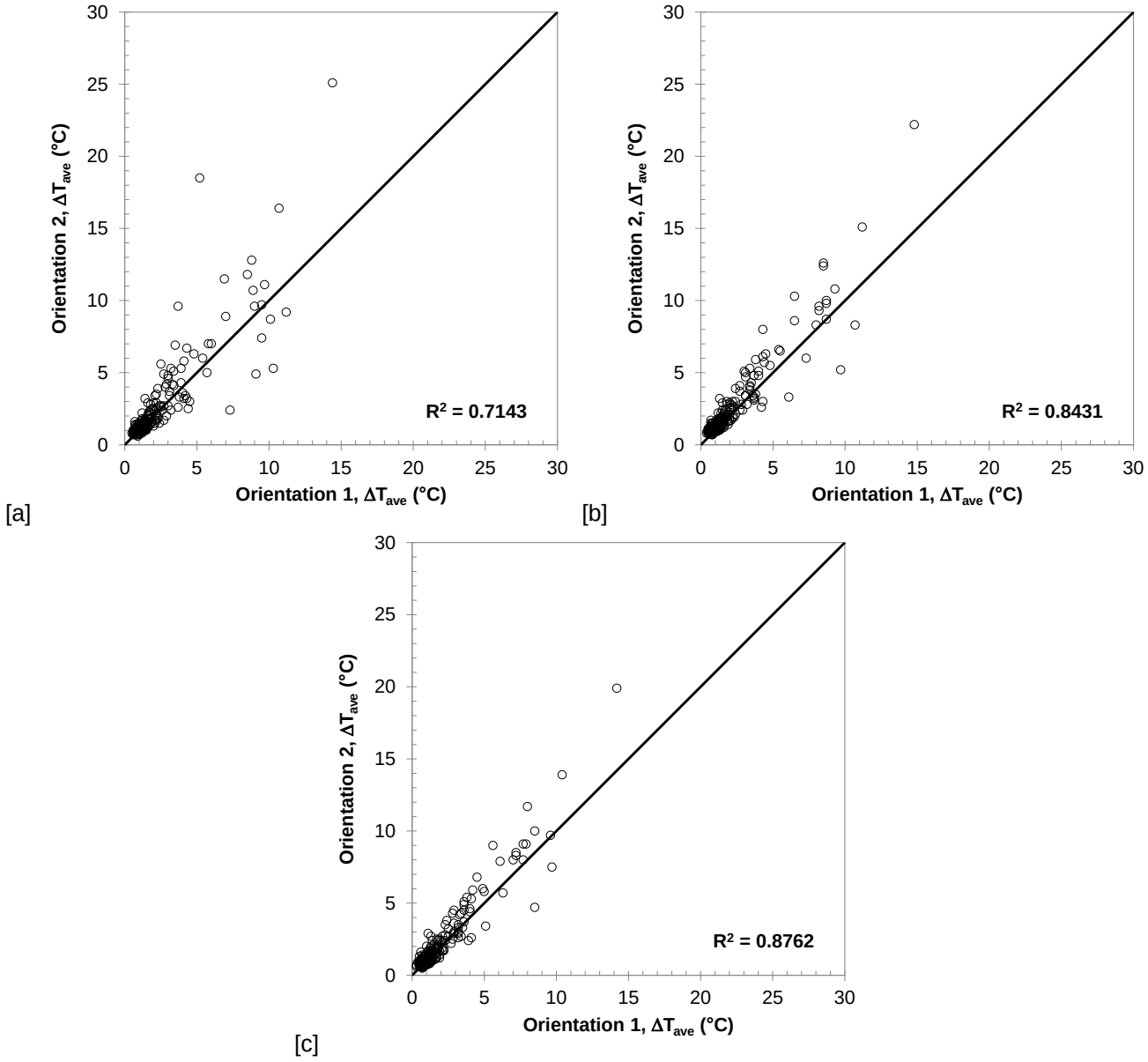

Figure 8: Sample #1 fragment thermal response for different orientations for [a] 20s, [b] 60s and [c] 120s thermal equilibrium times at ~1kWh/t

3.4 Thermal equilibration time

The effect of equilibration time following microwave treatment on the thermal response of the fragments is further illustrated in Figure 9 for sample #3 at approximately 1kWh/t. It can be seen that over a period of 20 to 120 seconds there was little change in average temperature rise for the majority of fragments. Fragments with a low average temperature rise, and therefore lesser amounts of microwave-absorbent material, exhibited negligible change over time, whereas the hotter fragments frequently exhibited a slightly higher or lower average temperature rise. A lower average temperature rise was observed when fragments contained surface mineralisation that could rapidly cool after microwave treatment. Conversely, a higher average temperature rise was observed for fragments that contained sub-surface mineralisation that required extra time for the internally generated heat to reach the surface of the fragment through conduction. These results on real ore fragments follow closely the observations made by John et al. (2015) on synthetic binary fragments, both numerically and experimentally. Therefore, it appears that thermal equilibration time would be unlikely to significantly affect sortability performance. However, it would still be important to select a thermal equilibrium time that matches any industrial sorting system to directly compare laboratory to industrial results.

http://dx.doi.org/10.1016/j.mineng.2016.07.007

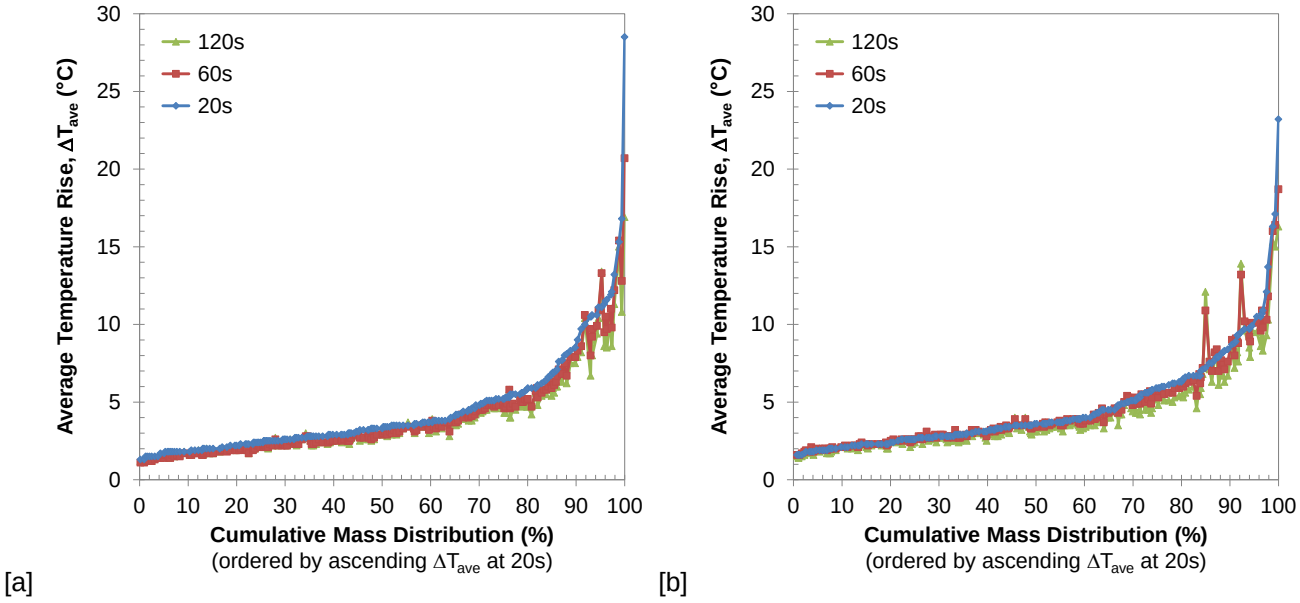

Figure 9: Sample #3 fragment thermal response at various equilibration times for [a] Orientation 1 and [b] Orientation 2 at ~1kWh/t

3.5 Fragment position in the cavity

To test the homogeneity of treatment across the cavity the fragments were arrayed in two different layouts by maintaining the row order but switching half the columns from one side of the belt to the other, illustrated in Figure 10. Repositioning the fragments in this way ensured that fragments occurring on the outside edge of the belt in the original layout (e.g. fragment #1 and #8) were switched the middle of the belt and vice versa.

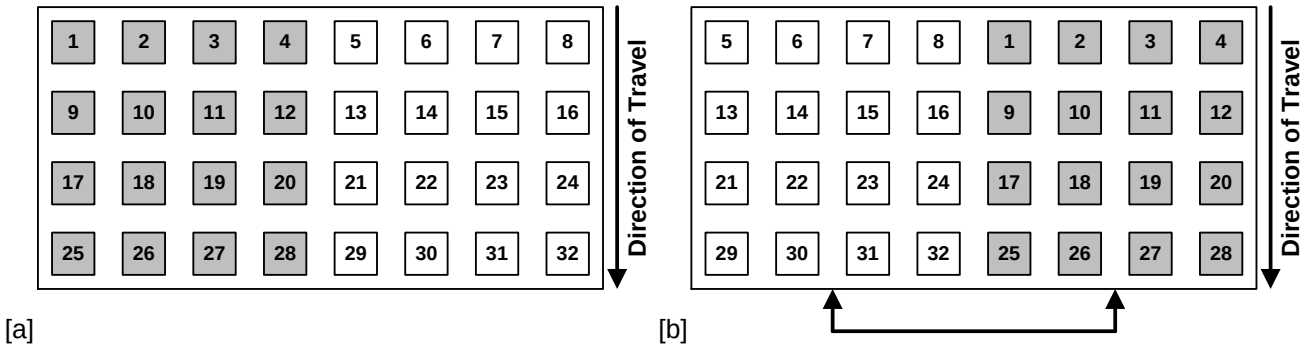

Figure 10: Fragment positioning in the cavity with [a] original layout and [b] "switch" layout

The effect of repositioning the fragments within the cavity on average temperature rise is illustrated for sample #11W at approximately 0.75kWh/t in Figure 11. It can be seen that on average there is little difference between the two layouts, particularly for the colder fragments with lesser microwave-absorbent material and for the -50.8+25.4mm size class (for which the cavity was designed to achieve ±20% with a homogeneous load). However, the -76.2+50.8mm and -25.4+12.7mm size classes demonstrated a fair amount of variability, particularly for the hotter fragments (>5°C).

The variability arises because the heterogeneous nature of mineralisation between individual fragments deviates from the homogeneous load used in the cavity design, which alters the electromagnetic field distribution within the cavity for different spacial distributions of microwave-heating phases and under different ore loading conditions. In other words, the more homogeneous the texture and load profile of an ore the less variation there would be as it trends towards the basis of design. In this respect, sample #11W may be considered as a "worst case scenario" as it contained a wide variety of textures with some fragments containing high total sulphide content (>10-20wt%) and others effectively microwave-heating phase barren.

Designing a system to support a higher instantaneous load within the cavity and an even more uniform electromagnetic field distribution would help to minimise such variations, so these observations are primarily a function of the belt-based pilot scale system used in these investigations. Importantly, in the vast majority of cases the difference in measured average temperature rise between layouts did not appear to make a hot fragment appear cold or vice versa, which might adversely affect sortability performance calculations when considering just

http://dx.doi.org/10.1016/j.mineng.2016.07.007

one fragment layout. The coefficient of determination (R^2) value for the observed data compared to the line of unity may be used as a measure of the thermal response variability, as shown in the figures.

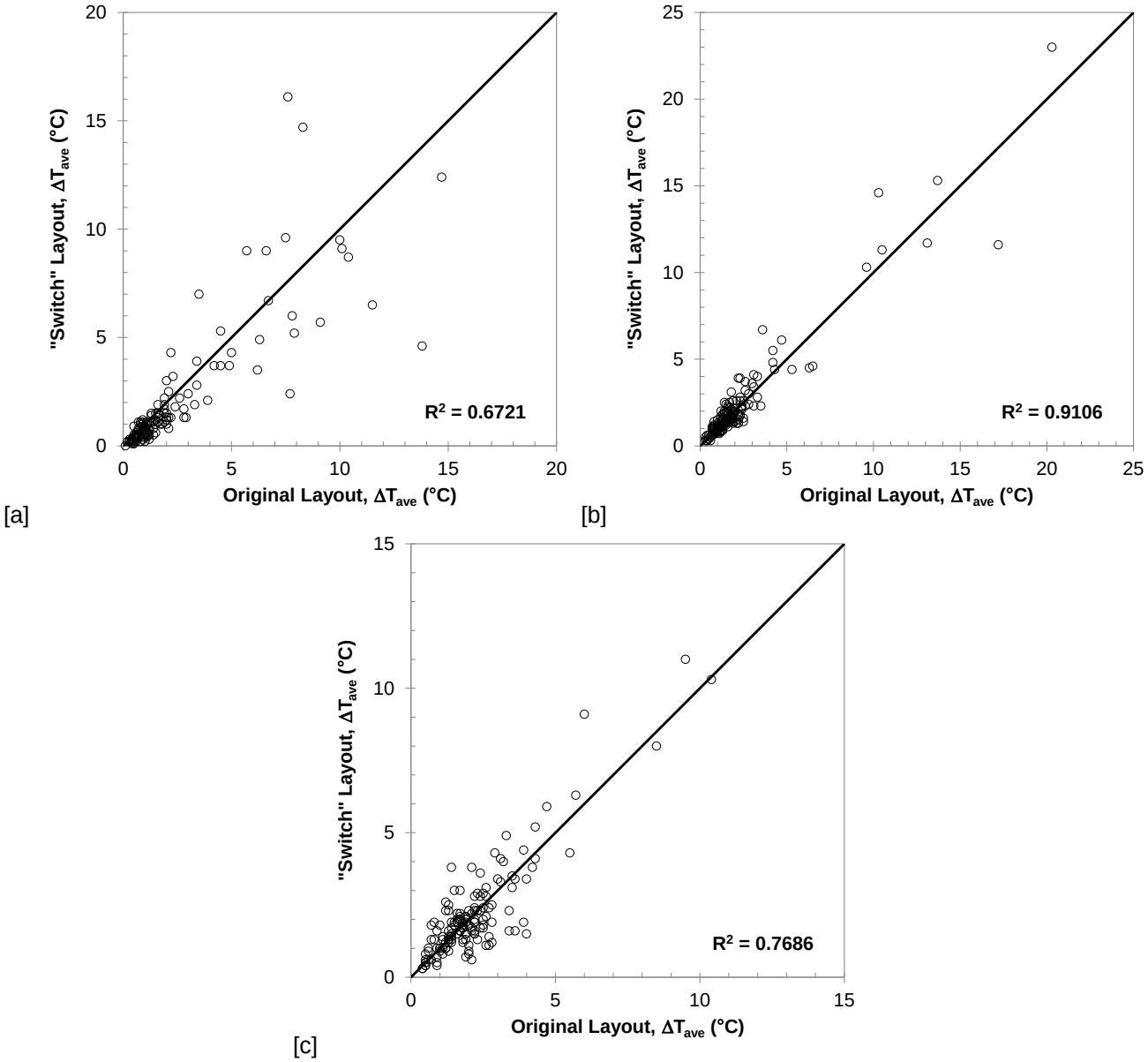

Figure 11: Sample #11W fragment thermal response due to position in the cavity for [a] -76.2+50.8mm, [b] -50.8+25.4mm and [c] -25.4+12.7mm size at ~0.75kWh/t

4 Ore sortability performance

4.1 Effect of dose on sortability

As mentioned previously, the microwave treatment energy dose is largely responsible for the ultimate temperature rise fragments experience. Figure 12a–c gives the average temperature rise plotted against copper content for sample #10, showing the thermal response over approximately 0.5–1.5kWh/t. Typically, the increased selectivity between hot and cold fragments did not significantly change the ordering of fragments from lowest to highest ΔT_{ave}. Therefore, there is usually little effect on the cumulative mass-copper sortability curves from which sortability performance is derived, illustrated in Figure 12d–f for samples #10, sample #10W and sample #4 respectively. The main role of dose is thus to provide enough separation between hot and cold fragments to overcome any error in discrimination (±°C) and physical separation to ensure an efficient sorting cut and minimise misreporting of fragments to different product streams.

http://dx.doi.org/10.1016/j.mineng.2016.07.007

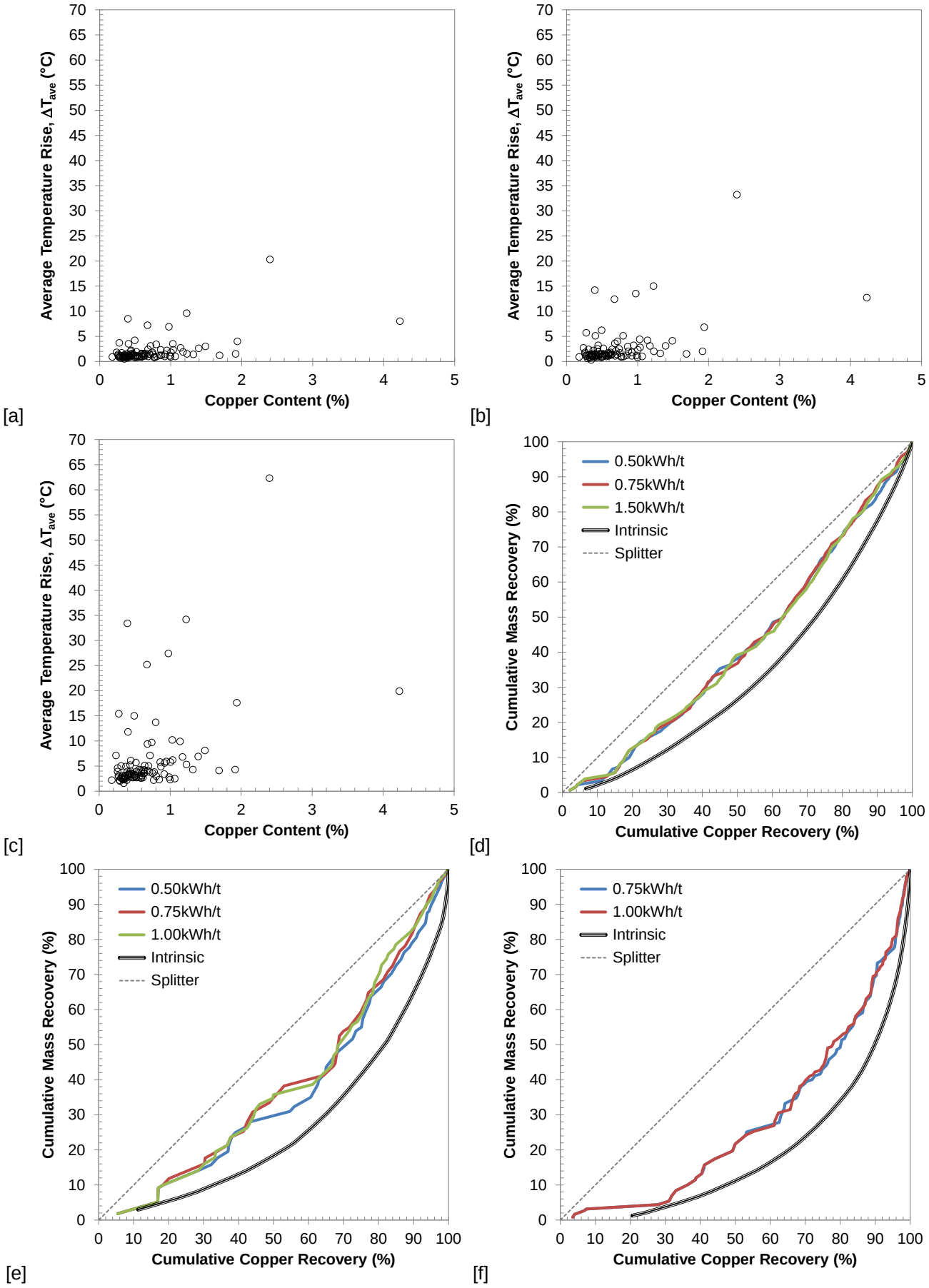

Figure 12: Sample #10 copper content versus average temperature rise at -50.8+25.4mm size at [a] ~0.5kWh/t, [b] ~0.75kWh/t and [c] ~1.5kWh/t; cumulative mass-copper recovery curves at -50.8+25.4mm size and variable dose for [d] sample #10, [e] sample #10W and [f] sample #4

http://dx.doi.org/10.1016/j.mineng.2016.07.007

4.2 Effect of fragment orientation on sortability

Figure 13a–c illustrates the variability in cumulative mass-copper recovery curves due to fragment orientation for sample #9W at -76.2+50.8mm, -50.8+25.4mm and -25.4+12.7mm size fragments respectively, at approximately 0.75kWh/t microwave treatment energy dose. Despite having a similar fragment thermal response variability between orientations as samples #1 and #9 presented previously, there was little difference in the sortability curves, particularly for the colder fragments (upper right end of the sortability curves).

The curves exhibited more divergence at the hotter end of the plots (lower left end of the curves) for the -25.4+12.7mm size fragments where the different orientations reordered some the fragments with a higher copper grade, which causes a sudden shift on the copper recovery axis relative to the mass recovery axis due to the higher proportion of total copper contained within these individual fragments. The total fragment surface average temperature rise (or average of both O1 and O2, denoted as O_{ave}) is also plotted and generally follows similar ordering compared to O1 or O2. In summary, while variability from fragment orientation may influence a potential cut-point when aiming to recover the hotter fragments, interrogating a single fragment orientation seems to generally be enough to determine the potential sortability of the ore as the ordering of fragments is close to the total surface measurement order.

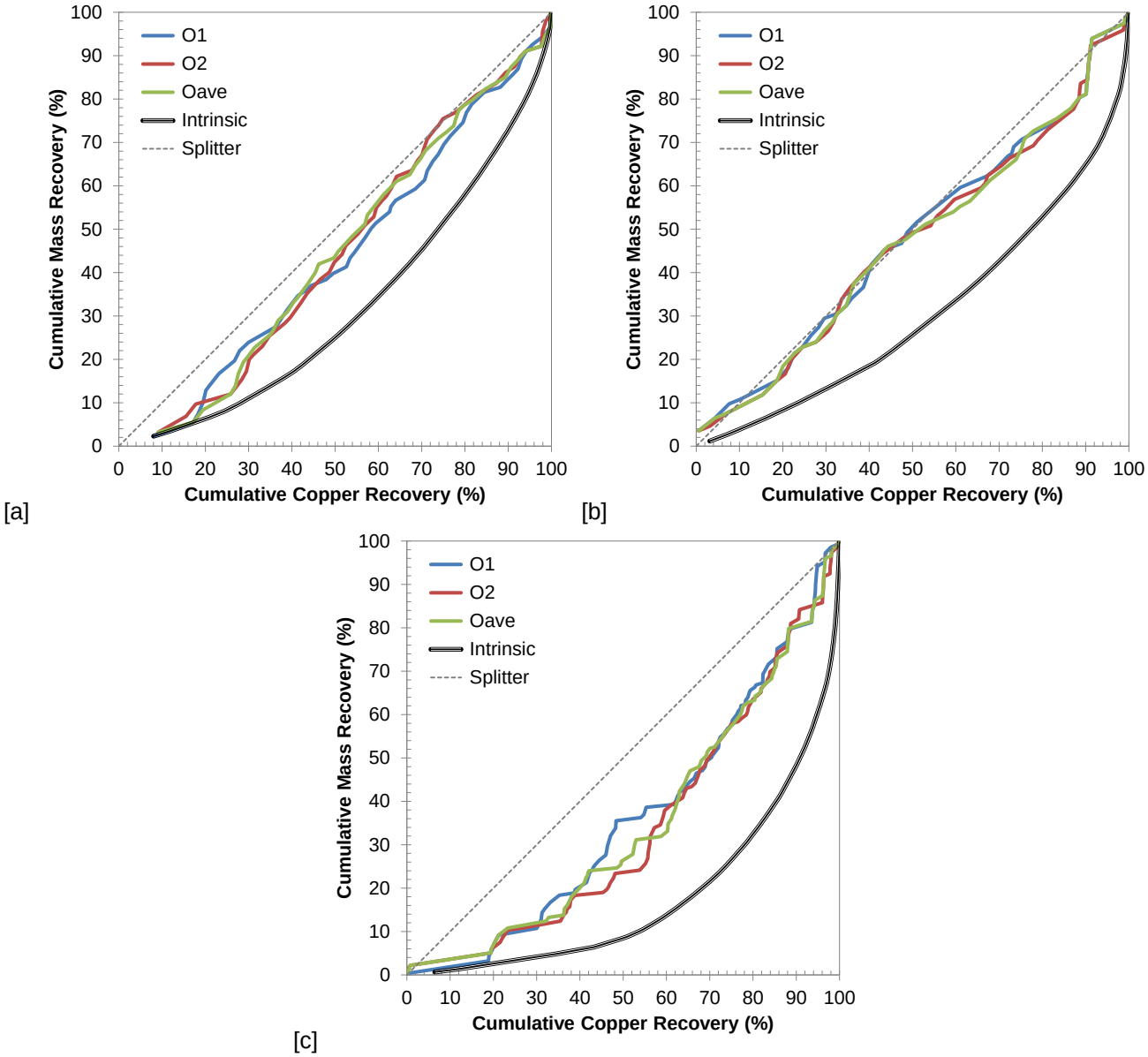

Figure 13: Sample #9W cumulative mass-copper recovery curves at different orientations for [a] -76.2+50.8mm, [b] -50.8+25.4mm and [c] -25.4+12.7mm size fragments at ~0.75kWh/t

http://dx.doi.org/10.1016/j.mineng.2016.07.007

4.3 Effect of thermal equilibration time sortability

Thermal equilibration over a period of 10–120 seconds was shown previously to have little effect on the average temperature rise of colder fragments, with few of the hotter fragments exhibiting a marked change in average temperature rise. The cumulative mass-copper recovery curves for sample #5 and sample #8W in Figure 14a–b respectively demonstrate that sortability performance was indeed only marginally affected by the amount of time fragments have had to cool following microwave treatment.

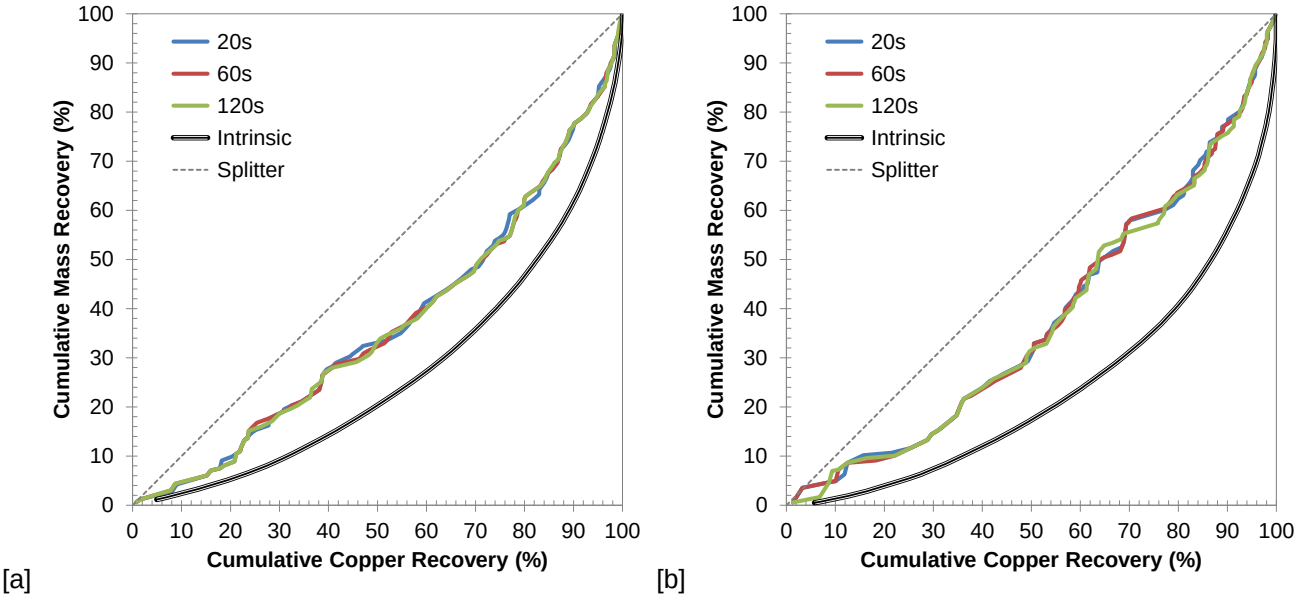

[a] [b]

Figure 14: Cumulative mass-copper recovery curves at variable thermal equilibration times for [a] sample #5 and [b] sample #8W at ~0.75kWh/t

http://dx.doi.org/10.1016/j.mineng.2016.07.007

4.4 Effect of fragment position in the cavity on sortability

Despite the larger observed variation in thermal response of hotter fragments (>5°C) due to position in the cavity, Figure 15a–c demonstrates that this variation did not adversely affect the cumulative mass-copper recovery curves for sample #11W because it did not change the response of individual fragments from hot to cold or vice versa.

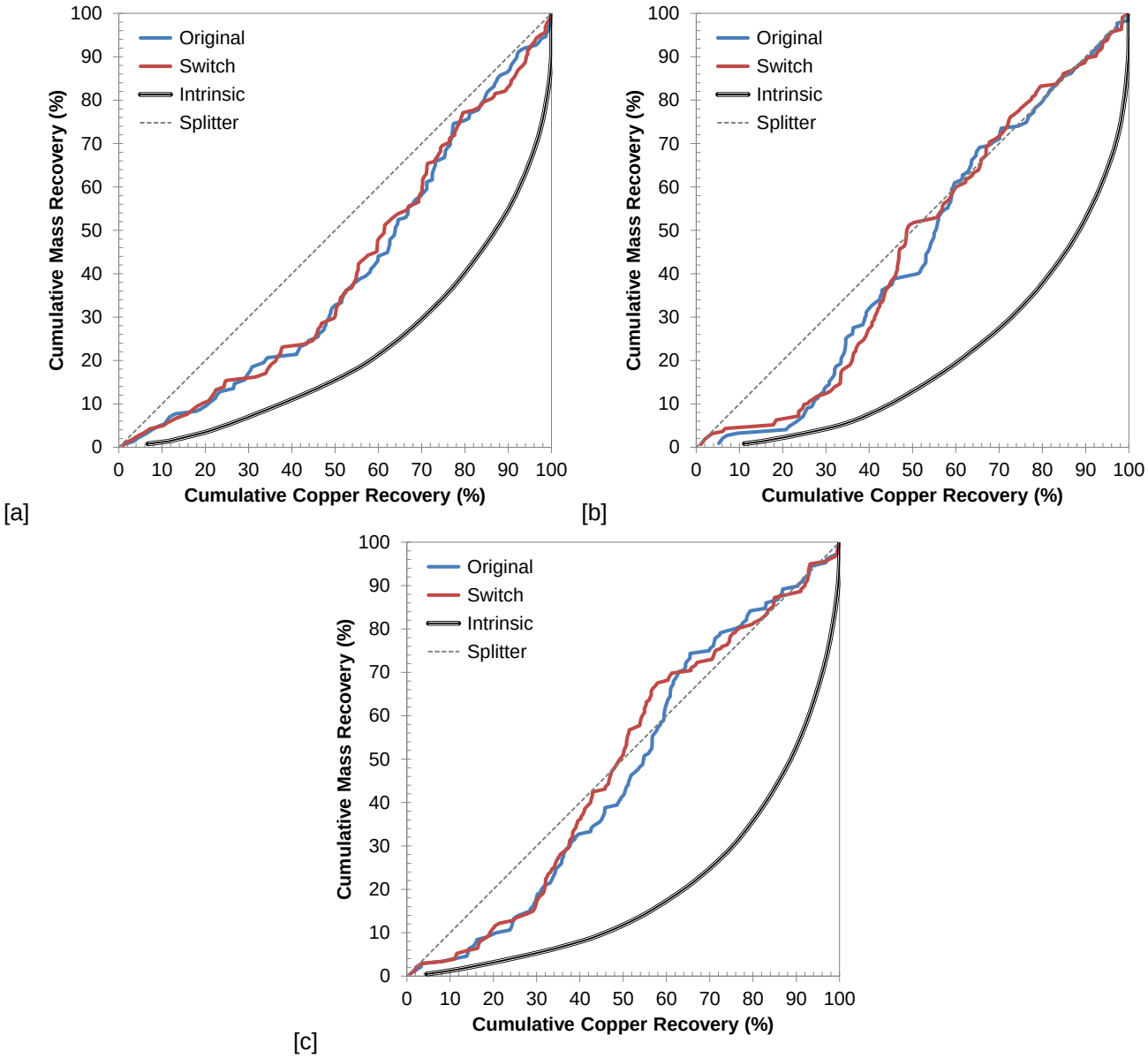

Figure 15: Sample #11W cumulative mass-copper recovery curves due to position in the cavity for [a] -76.2+50.8mm at ~0.5kWh/t, and [b] -50.8+25.4mm and [c] -25.4+12.7mm size fragments at ~0.75kWh/t

4.5 Effect of sample size on sortability

The effect of sample size (number of fragments) on the variability of the sortability curves is given in Figure 16 for sample #11W. Sample #11W may be considered to be a potential “worst case scenario” because it contained a relatively small proportion of hot fragments (>5°C) and also contained one or two fragments per 100 that had a higher than usual copper content, individually contributing approximately 5–10% of the total copper within the sample. Both of these characteristics can cause the sortability curves to suddenly shift depending on where these fragments fall in the hottest to coldest order. While samples with a more contiguous range of fragment copper content values did not suffer from this phenomenon, it can also be mitigated to some extent by increasing the sample size.

http://dx.doi.org/10.1016/j.mineng.2016.07.007

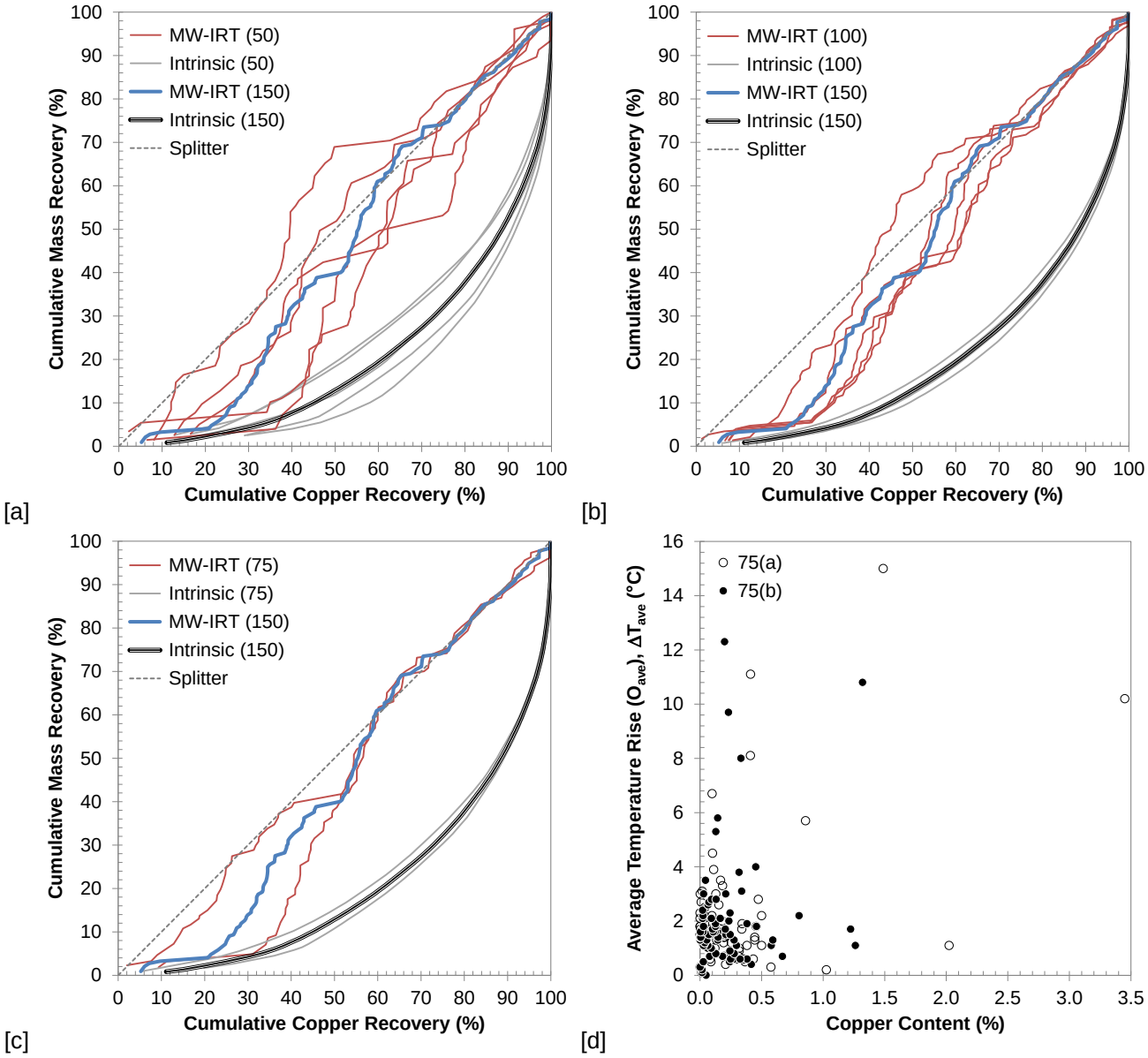

Figure 16: Sample #11W effect of sample size on sortability for [a] 50 versus 150 fragments, [b] 100 versus 150 fragments and [c] 75 versus 150 fragments at -50.8+25.4mm size (O2) and ~0.75kWh/t; [d] copper content versus ΔT_{ave} for 75 versus 150 fragments

The data was split into five random groups of either 50 fragments or 100 fragments (simulating representative subdivision of the original sample) and the sortability curves compared to that of the original 150 fragment sample. It is clearly seen that there was significantly more variability in both the intrinsic and MW–IRT sortability curves when considering only 50 fragments, whereas 100 fragments provided a closer representation of the sample, particularly for intrinsic sortability.

The sample was then split into two groups of 75 fragments by selecting every second fragment on a ΔT_{ave} basis when ordered from coldest to hottest. It can be seen that for the colder fragments, where there are many fragments with similar ΔT_{ave} and copper content, the MW–IRT and intrinsic curves are very close to that provided by 150 fragments. The curves diverge for the hotter fragments for the reasons described in the previous paragraphs of this section. Nevertheless, selecting every second fragment on a temperature rise basis appears to be a better method for selecting a sub-sample for analysis.

The effect of sample size on the variability of the sortability performance values is summarised in Table 7. Again, it can be seen that the largest variation is present when selecting only 50 fragments, with an average absolute difference of approximately 18–22%, compared to selecting 100 fragments, with an average absolute difference of approximately 10–15%. Selecting every second fragment on a ΔT_{ave} basis gave an average absolute difference of approximately 1.6% for P_{75} and P_{50}, and 16% for P_{25}. Therefore, while it will always be the most desirable to test as many fragments as time and budget will permit to improve the test sample representivity, it is recommended that a minimum of 100 fragments be considered for this type of testing in future.

http://dx.doi.org/10.1016/j.mineng.2016.07.007

Table 7

Difference in sortability performance due to sample size

Sample Size	P_{XX} Difference (%)		
	P_{25}	P_{50}	P_{75}
150 Fragments	22.8	13.8	6.2
50 Fragments			
Set A	-21.7	-39.6	-31.9
Set B	+21.1	+13.5	+25.7
Set C	+9.2	+20.4	-7.2
Set D	+24.9	+12.4	+32.1
Set E	+12.4	-23.3	-4.5
Average*	(17.9)	(21.8)	(20.3)
100 Fragments			
Set A	+6.5	-3.5	-0.8
Set B	-1.6	+10.7	-6.8
Set C	+15.3	+18.2	+13.3
Set D	+20.0	+18.2	+14.4
Set E	-5.6	-27.0	-16.7
Average	(9.8)	(15.5)	(10.4)
75 Fragments			
Set A	+10.8	-0.4	-1.6
Set B	-22.1	+3.0	-1.5
Average	(16.5)	(1.7)	(1.6)

* () denotes average absolute difference

4.6 MW–IRT versus intrinsic copper sortability

The sortability performance of the ores tested can broadly be categorised into good sortability (>75%), moderate sortability (50–75%) and poor sortability (<50%) (or other categories depending on economic considerations for a particular mine site). A selection of ores in each category with the 25% mass rejections (i.e. accepting the hottest 75% by mass) are presented in Table 8 with the corresponding copper content versus ΔT_{ave} and cumulative mass-copper recovery curves presented in Figure 17, Figure 18 and Figure 19.

Table 8

Separations at -50.8+25.4mm size and 25% mass rejection for selected samples

Parameter	Units	Good		Moderate		Poor	
		#2	#7	#5	#10	#12	#11W
Feed							
Copper Grade	%	2.091	0.733	0.559	0.707	0.365	0.260
I_{75}		1.22	1.26	1.28	1.18	1.32	1.30
P_{75}	%	90.0	84.2	68.9	55.6	25.2	3.2
ΔT_{ave} Cut Point	°C	<2.1	<1.8	<2.1	<1.4	<0.6	<1.2
Accepts (Hots)							
Copper Grade	%	2.513	0.891	0.666	0.778	0.395	0.262
Copper Upgrade		1.20	1.22	1.19	1.10	1.08	1.01
Copper Recovery	%	90.0	90.6	88.5	82.5	80.5	75.8
Mass Yield	%	74.9	74.6	74.4	75.0	74.6	75.1
Rejects (Colds)							
Copper Grade	%	0.834	0.270	0.251	0.495	0.280	0.252
Copper Recovery	%	10.0	9.4	11.5	17.5	19.5	24.2
Mass Yield	%	25.1	25.4	25.6	25.0	25.4	24.9

http://dx.doi.org/10.1016/j.mineng.2016.07.007

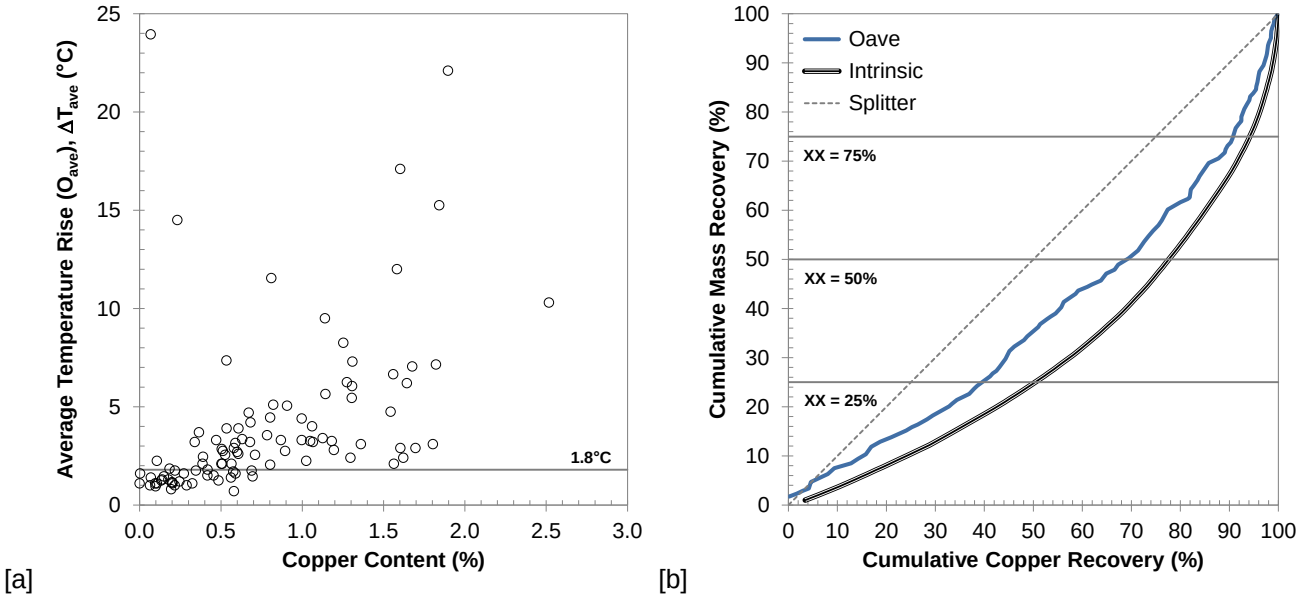

Figure 17: Sample #7 "good" ore sortability example at ~1kWh/t [a] copper versus average temperature rise and [b] cumulative mass-copper recovery curves

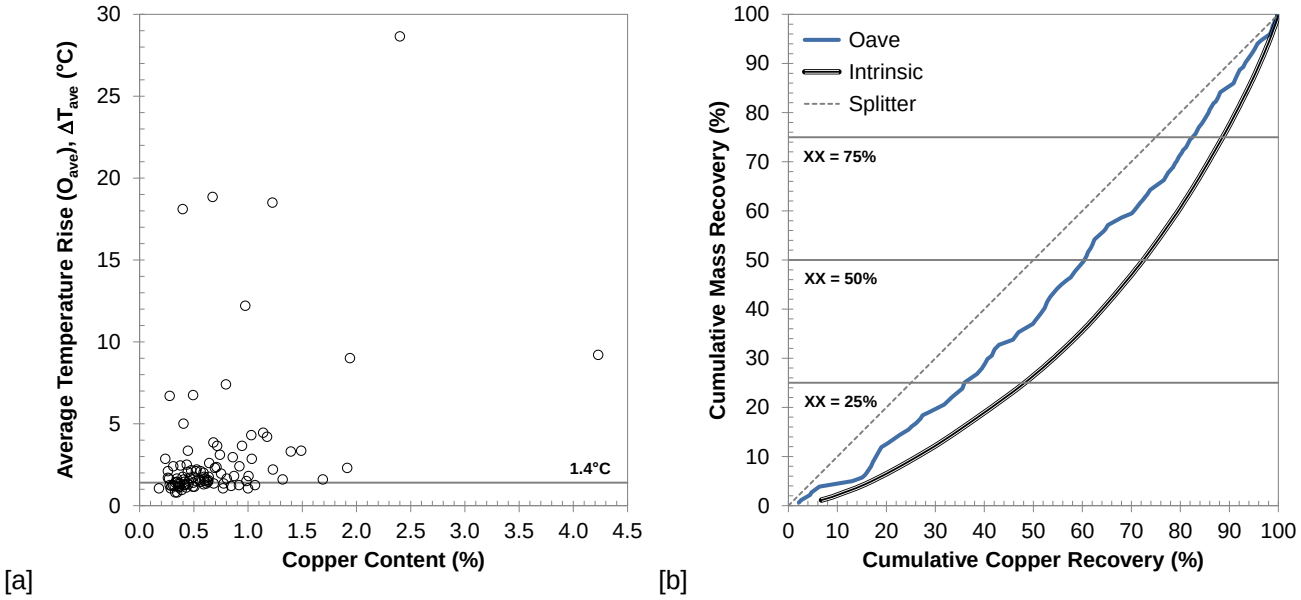

Figure 18: Sample #10 "moderate" ore sortability example at ~0.75kWh/t [a] copper versus average temperature rise and [b] cumulative mass-copper recovery curves

http://dx.doi.org/10.1016/j.mineng.2016.07.007

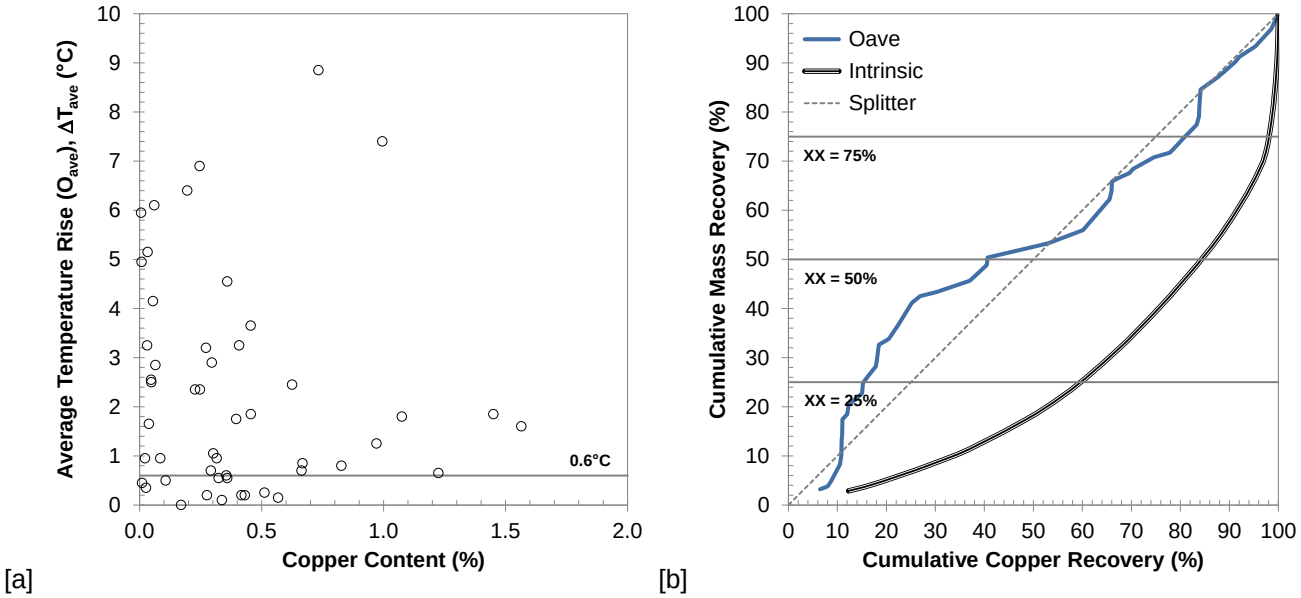

Figure 19: Sample #12 "poor" ore sortability example at ~0.75kWh/t [a] copper versus average temperature rise and [b] cumulative mass-copper recovery curves

By collating all of the sortability data for the 16 ores tested, a sortability map of the sorting potential (intrinsic) versus the sortability performance by MW–IRT at different mass rejections may be plotted to compare different samples, illustrated in Figure 20a/c/e. The data is also presented in Table S.3 in the Supplementary Information for reference. The samples may also be plotted as a ranking against the testing percentile, as shown in Figure 20b/d/f. The testing percentile is presented as the percent number of samples tested for this campaign but may also be represented as a mass percentage, for example to compare the sortability of different ore types against a mine plan.

http://dx.doi.org/10.1016/j.mineng.2016.07.007

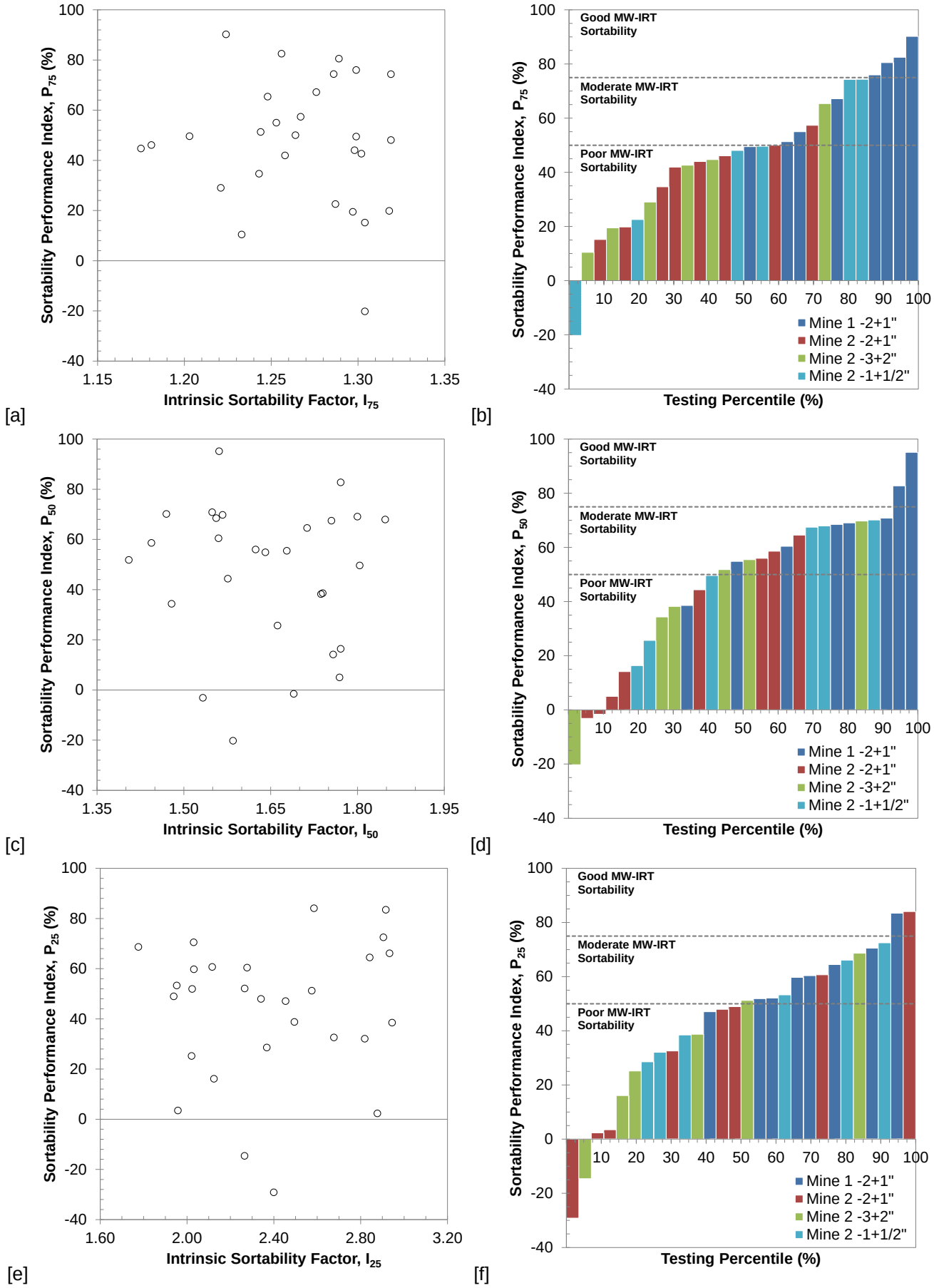

Figure 20: Sortability maps for accepting the hottest [a] 75%, [c] 50% and [e] 25% by mass; sortability rankings by testing percentile for accepting the hottest [b] 75%, [d] 50% and [f] 25% by mass

http://dx.doi.org/10.1016/j.mineng.2016.07.007

Arbitrary mass rejections may be useful for ranking or comparing ores but when considering a separation for upgrading metal values it is better to consider the thermal response for each ore separately. Table 9 compares the 25% mass rejection against tailored sorting cut points for three ores, with the corresponding copper content versus ΔT_{ave} and cumulative mass-copper recovery curves presented in Figure 21, Figure 22 and Figure 23. It can be seen that by altering the temperature cut point the copper grade of the rejects can be more closely controlled, thereby optimising the copper recovery to accepts and mass rejection to the rejects depending on the most economic benefit for the ore. The potential separations for sample #11 also demonstrated that a dual cut point may be employed to selectively reject a middlings (by average temperature rise) stream, which maintained upgrade ratio but increased copper recovery to accepts and reduced rejects grade compared to a single temperature separation.

Table 9

Potential separations at -50.8+25.4mm size for selected samples

Parameter	Units	#1			#11			#8W		
Feed										
Copper Grade	%	0.385	0.385	0.385	0.265	0.265	0.265	0.046	0.046	0.046
$I_{75(25)}$		1.30	-	-	1.29	-	-	1.30	(1.71)	-
$P_{75(25)}$	%	82.7	-	-	45.1	-	-	63.9	(49.1)	-
ΔT_{ave} Cut Point	°C	<1.2	<1.1	<1.4	<1.5	<2.2	1.3-2.2	<1.4	<2.4	<7.0
Accepts (Hots)										
Copper Grade	%	0.480	0.447	0.551	0.300	0.391	0.398	0.055	0.079	0.094
Copper Upgrade		1.25	1.16	1.43	1.13	1.47	1.50	1.19	1.71	2.04
Copper Recovery	%	93.7	95.9	87.2	85.5	72.6	84.4	89.3	44.2	22.9
Mass Yield	%	74.9	82.6	60.9	75.5	49.2	56.3	75.0	25.8	11.2
Rejects (Colds)										
Copper Grade	%	0.102	0.091	0.126	0.157	0.143	0.095	0.020	0.035	0.040
Copper Recovery	%	6.6	4.1	12.8	14.5	27.4	15.6	10.7	55.8	77.1
Mass Yield	%	25.1	17.4	39.1	24.5	50.8	43.7	25.0	74.2	88.8

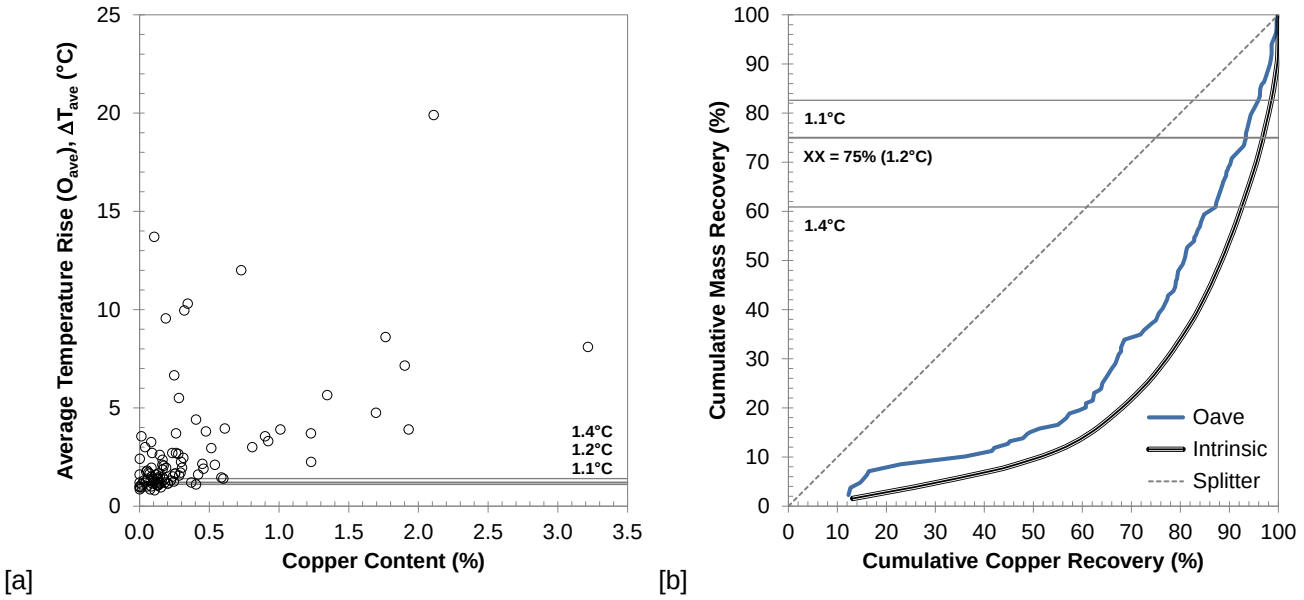

[a] [b]

Figure 21: Sample #1 sortability at ~1kWh/t [a] copper versus average temperature rise and [b] cumulative mass-copper recovery curves

http://dx.doi.org/10.1016/j.mineng.2016.07.007

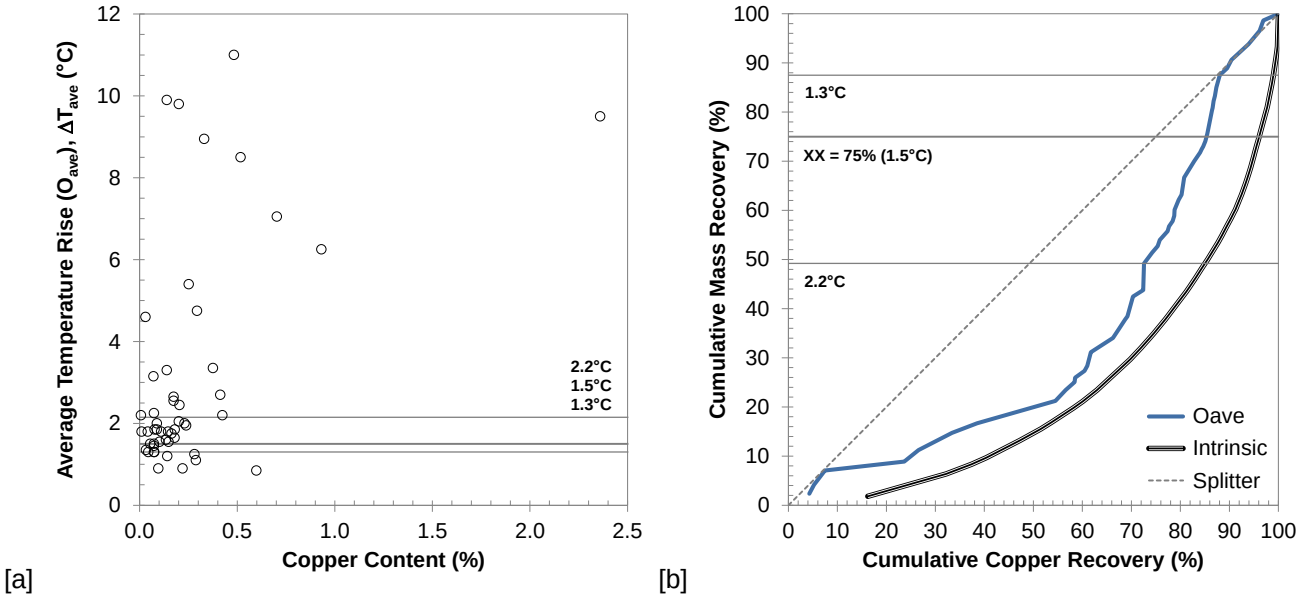

Figure 22: Sample #11 sortability at ~0.75kWh/t [a] copper versus average temperature rise and [b] cumulative mass-copper recovery curves

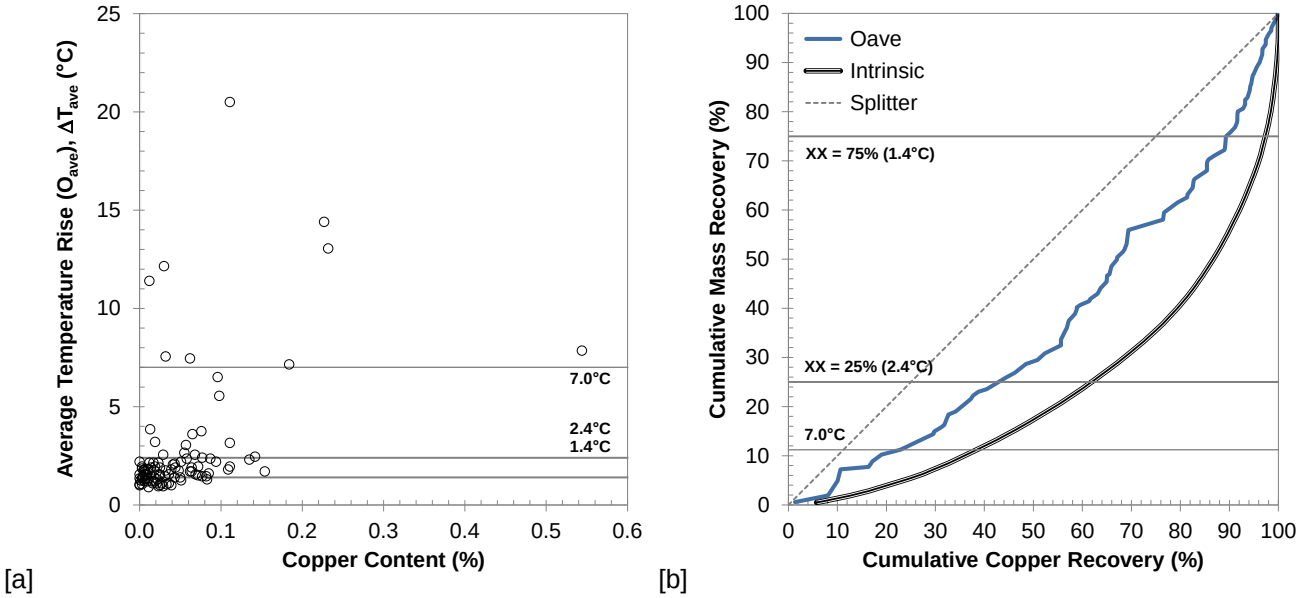

Figure 23: Sample #8W sortability at ~0.75kWh/t [a] copper versus average temperature rise and [b] cumulative mass-copper recovery curves

http://dx.doi.org/10.1016/j.mineng.2016.07.007

5 The influence of gangue mineralogy on thermal response

From the data presented in the previous sections it is apparent that intrinsic or near-intrinsic sortability is not achievable for many of the ores tested using the MW–IRT method. The effects of power density distribution within the cavity, heterogeneity of fragments textures, dissemination of microwave-heating phases within each fragment (i.e. the effect of orientation) and other operating conditions have been shown to have only marginal effects on the sortability of the ores. The most important aspect with respect to sortability performance is the influence of microwave-heating gangue minerals.

As shown in the modal mineralogy tables, the microwave-heating gangue minerals predominantly include iron and other minor sulphides, iron and titaniferrous oxides, and water contained within hydrated clays. Hygroscopic moisture may also be present in addition to that contained within the hydrated clays, both of which were accounted for during moisture content determination. Chemical assays were able to determine copper, sulphur and iron content; however, the iron oxide content could not be determined due to iron being present in many non microwave-heating gangue minerals. The quartzite ores from Mine 2 contained very little iron-bearing non-heaters, so the iron content was mostly attributable to iron oxides and sulphides.

Figure 24a–e, Figure 25a–e, Figure 26a–e and Figure 27a–e give ΔT_{ave} versus copper, sulphur, moisture, iron and total heating phase content for samples #9, #10, #11 and #6 respectively. It can be seen for all three lithology types from Mine 2 that moisture content is the most significant phase contributing to heating for low ΔT_{ave} (<5°C) fragments, even when the sulphide content is up to approximately 2–3 times greater than moisture. High ΔT_{ave} (>5°C) fragments are largely driven by high total sulphide content, where the sulphide content is greater than approximately 2–3 times that of moisture. For Mine 1, copper and iron sulphides tend to dominate heating.

Figure 24f, Figure 25f, Figure 26f and Figure 27f give the intrinsic and MW–IRT sortability curves compared to the copper sortability based on total microwave-heating phase content. In general, it can be seen that the total heating phase curve more closely approximates the MW–IRT sortability curves, as would be expected. The three curves would typically be closer to each other when there was a high copper sulphide to iron sulphide ratio and/or good correlation between copper and iron sulphide content (i.e. co-mineralisation). However, since water is an excellent microwave-heating phase, low moisture content ores were more likely in general to achieve better sortability performance, particularly for low ΔT_{ave} separations (i.e. $P_{>50}$) as shown in Figure 28.

It is apparent from the previous plots that summing the total microwave-heating phases does not give a good fit to ΔT_{ave} despite illustrating that increasing microwave-heating phase content does indeed result in a higher temperature rise. This is partly due to fragment texture and sample heterogeneity effects described previously, but also due to the fact that different minerals have different heating rates under microwave irradiation, thereby contributing to heating in different proportions. It is also true that the same minerals from different mine sites and potentially from different regions within the same mine may have stoichiometric defects or differences that may influence heating rates. All of these considerations contribute to the degree of scatter observed in the plots.

Furthermore, some of the fragments appeared to achieve a higher temperature rise than the total microwave-heating phase content would otherwise suggest. A subsequent analysis identified that these fragments contained a significant proportion (up to approximately 10%) of highly magnetic minerals, predominantly magnetite, and weakly magnetic minerals (up to approximately 25%), predominantly garnets. Highly magnetic materials heat exceptionally well in microwaves and the omission of magnetics as a separate assay should be rectified in any future testing programme. Full characterisation of all heating phases may then potentially allow the contributions to heating to be weighted by phase for a particular mine or ore sample.

http://dx.doi.org/10.1016/j.mineng.2016.07.007

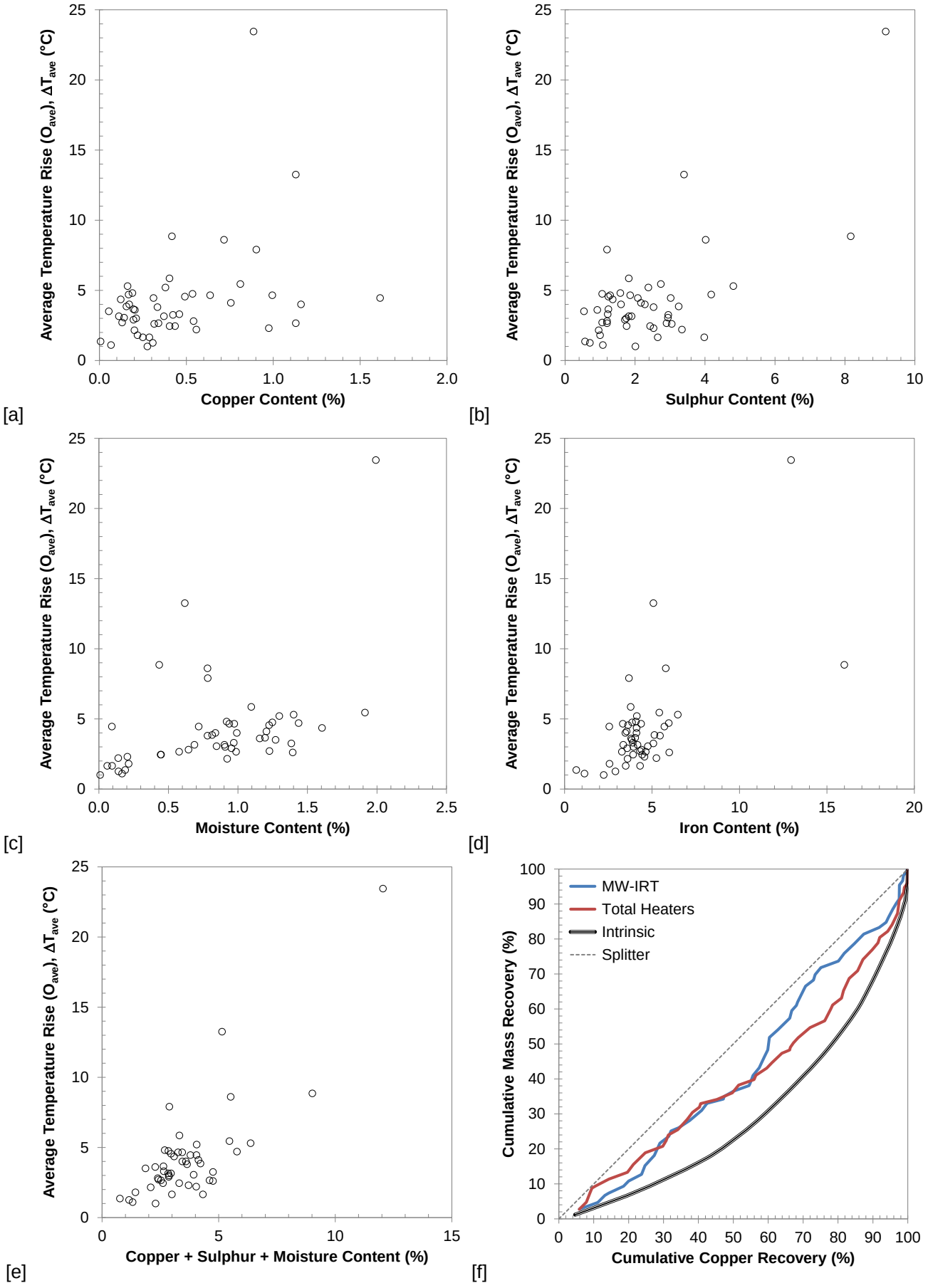

Figure 24: Sample #9 -50.8+25.4mm size treatment at ~1kWh/t [a] copper versus ΔT_{ave}, [b] sulphur versus ΔT_{ave}, [c] moisture versus ΔT_{ave}, [d] iron versus ΔT_{ave}, [e] total heating phase content versus ΔT_{ave} and [f] cumulative mass-recovery curves

http://dx.doi.org/10.1016/j.mineng.2016.07.007

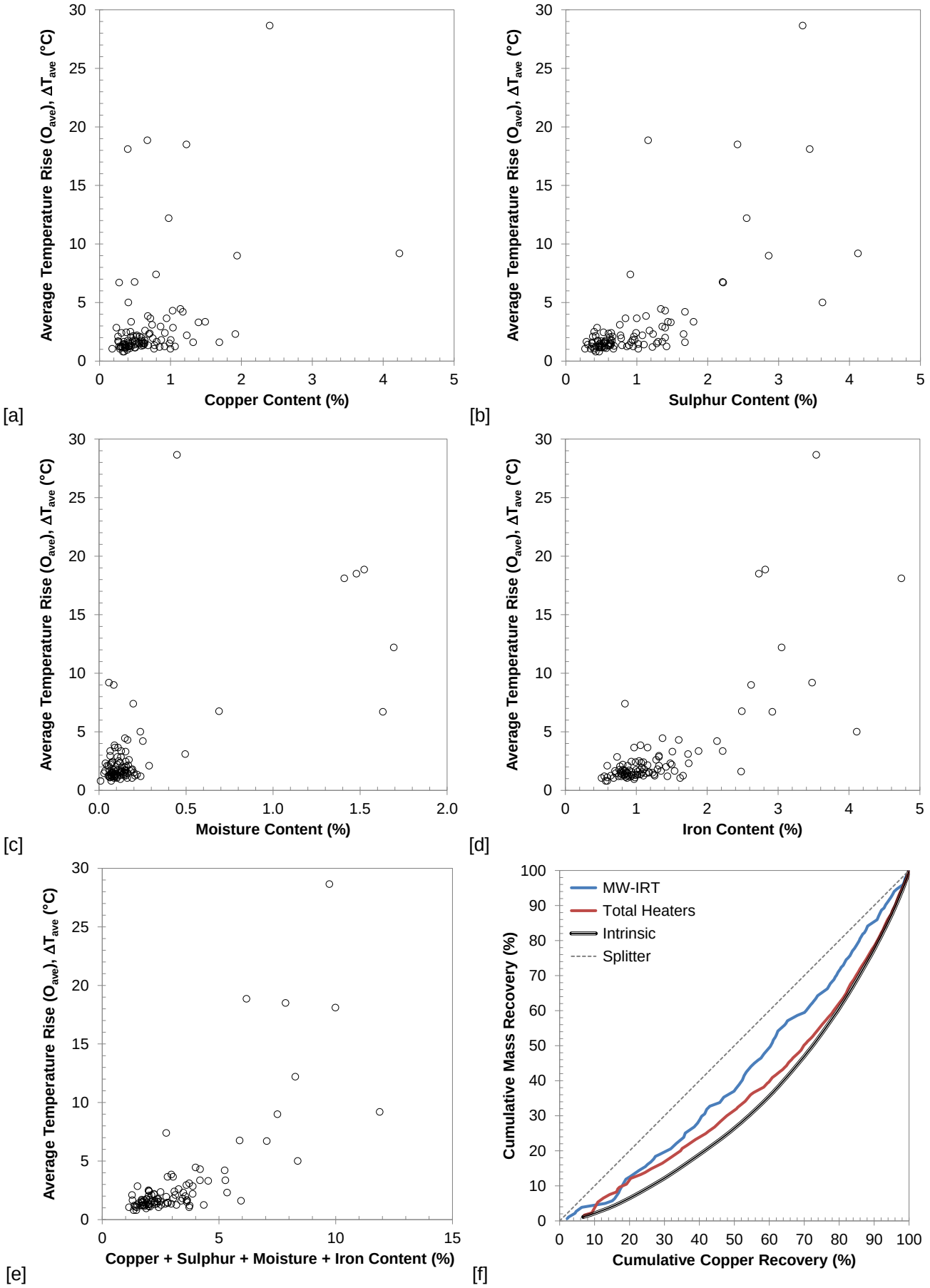

Figure 25: Sample #10 -50.8+25.4mm size treatment at ~0.75kWh/t [a] copper versus ΔT_{ave}, [b] sulphur versus ΔT_{ave}, [c] moisture versus ΔT_{ave}, [d] iron versus ΔT_{ave}, [e] total heating phase content versus ΔT_{ave} and [f] cumulative mass-recovery curves

http://dx.doi.org/10.1016/j.mineng.2016.07.007

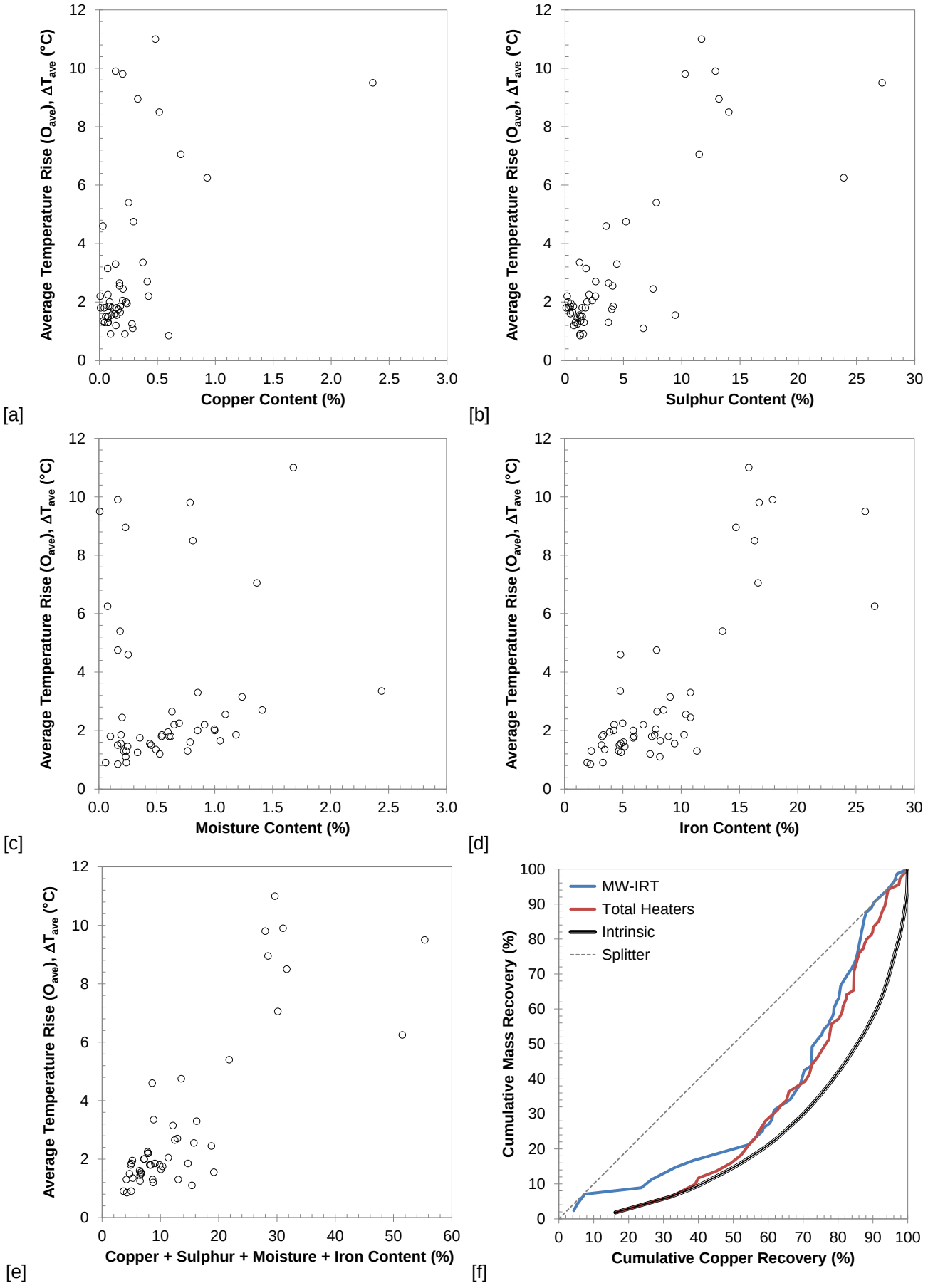

Figure 26: Sample #11 -50.8+25.4mm size treatment at ~0.75kWh/t [a] copper versus ΔT_{ave}, [b] sulphur versus ΔT_{ave}, [c] moisture versus ΔT_{ave}, [d] iron versus ΔT_{ave}, [e] total heating phase content versus ΔT_{ave} and [f] cumulative mass-recovery curves

http://dx.doi.org/10.1016/j.mineng.2016.07.007

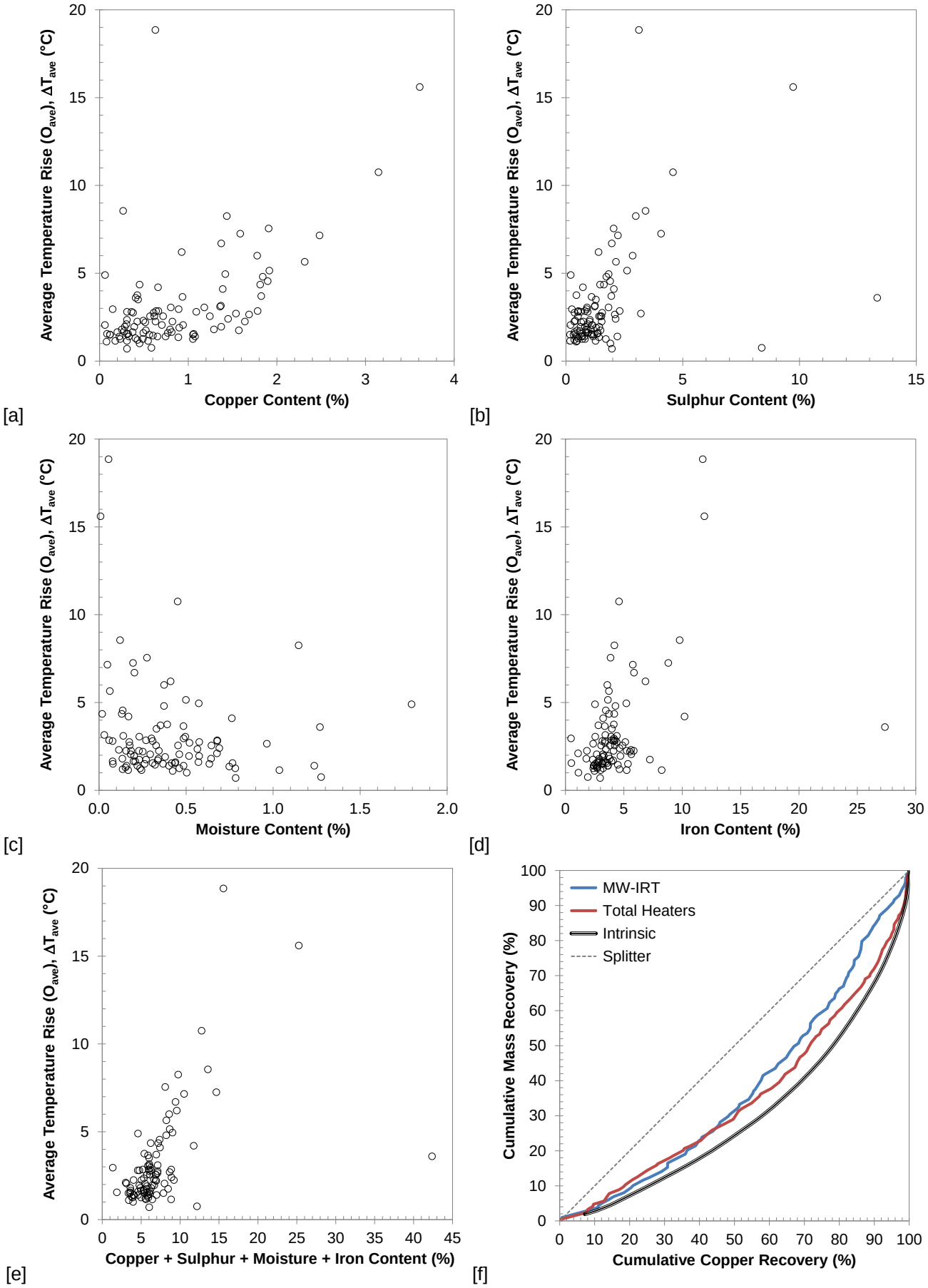

Figure 27: Sample #6 -50.8+25.4mm size treatment at ~0.75kWh/t [a] copper versus ΔT_{ave}, [b] sulphur versus ΔT_{ave}, [c] moisture versus ΔT_{ave}, [d] iron versus ΔT_{ave}, [e] total heating phase content versus ΔT_{ave} and [f] cumulative mass-recovery curves

http://dx.doi.org/10.1016/j.mineng.2016.07.007

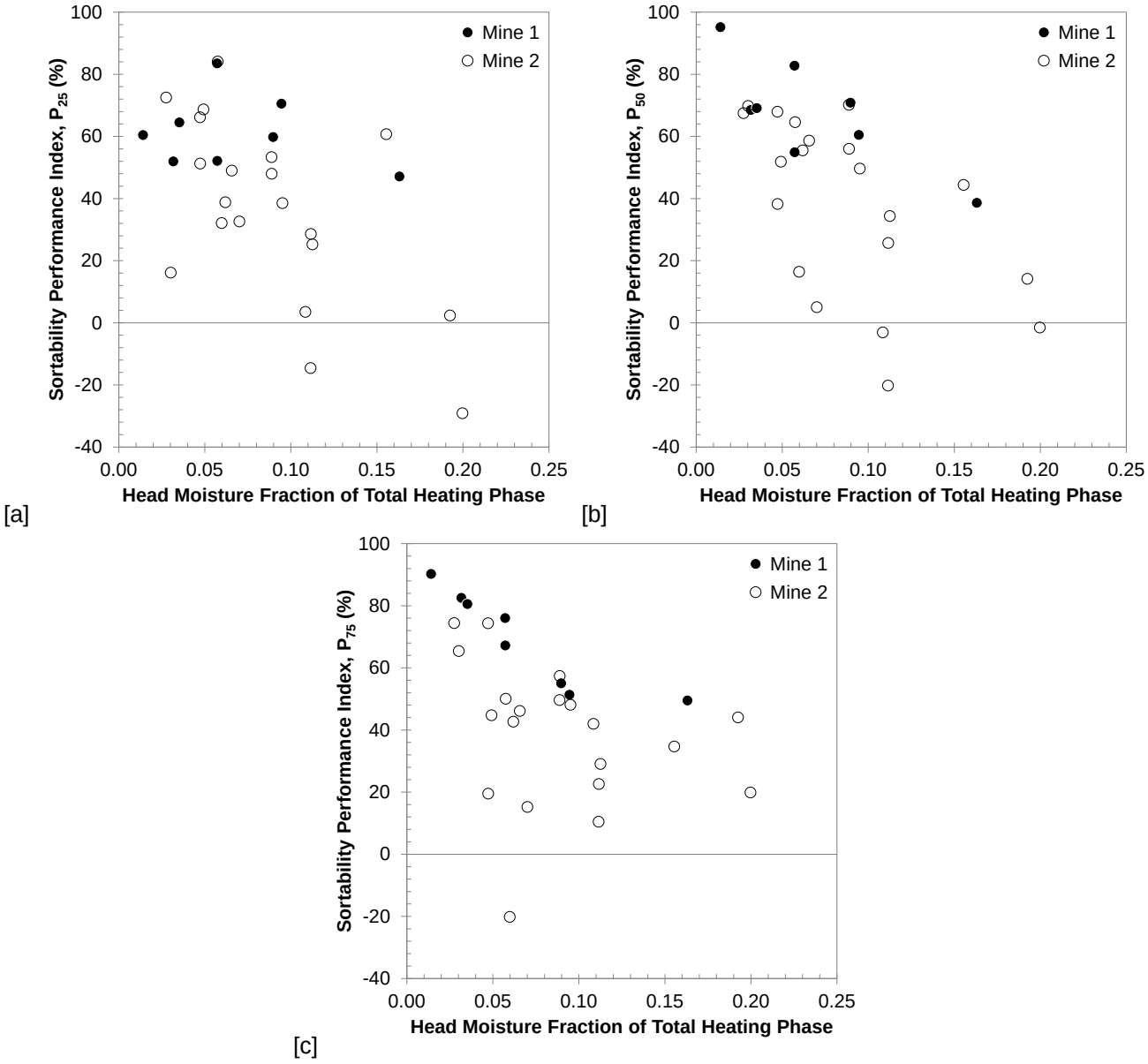

Figure 28: Sortability performance versus head moisture fraction of total microwave-heating phase for [a] P_{25}, [b] P_{50} and [c] P_{75}

http://dx.doi.org/10.1016/j.mineng.2016.07.007

6 Conclusions

A bespoke pilot scale microwave treatment system operating batch wise in a laboratory environment has been evaluated for fragment-by-fragment sorting of porphyry copper ores. The microwave cavity was shown to provide a sufficiently homogeneous field such that the fragment temperature rise was a function of mineralogy and not a function of a variable field pattern.

Microwave treatment energy dose was found to be the driving force behind the ultimate average temperature fragments experience, with other process variables (e.g. belt speed, power, belt mass loading, thermal equilibration time) having little effect on sortability performance. Therefore, as a basis of design for an industrial system, it would be recommended to perform treatments at the minimum energy required to effect a valuable separation with the highest practical power and flow velocity to maximise throughput.

The presence of microwave-heating gangue minerals (e.g. iron sulphides, iron oxides and hydrated clays) was shown to be the dominant source of deviation from intrinsic sortability. However, low average moisture content and co-mineralisation of copper and iron sulphides (or bulk sulphide sorting) was found to mitigate the deviation and provide better sortability performance. While fragment mineralogical texture and ore textural heterogeneity were shown to influence the average temperature rise of the fragment surface presented to the thermal camera, in most cases this variability did not adversely affect sortability performance.

The MW–IRT sorting technique presented was not meant to be a diagnostic tool for the accurate determination of fragment-by-fragment copper grade, but rather to provide a means to discriminate fragments with higher or lower copper content to form the basis of a potential separation. In this respect, an attractive separation could be proposed for many of the ores tested, either to remove a large proportion of barren fragments from ore-grade material or concentrate a large proportion of copper values from waste-grade material.

A final reflection on the testing methodology would also lend the authors to consider that a minimum of at least 100 fragments should be chosen for any future testing, preferably more (potentially up to 200 fragments) if time and budget allow. The increase in representivity achieved by taking a larger sample size allows for the inclusion of more mineralogy combinations to identify different heating groups and smooths out the sortability performance curves by incorporating a more contiguous range of copper assay values, eliminating large shifts in cumulative mass and copper recovery values.

Acknowledgements

The authors greatly acknowledge Rio Tinto Technology and Innovation along with their research and industry partners for engagement and collaboration throughout the Copper NuWave™ project.

http://dx.doi.org/10.1016/j.mineng.2016.07.007

References

Adair, B., Morrison, R., Kanchibotla, S., 2013. Implications of next generation ore sorting for definition of an ore deposit, Physical Separation'13. Minerals Engineering International, Falmouth, June.

Ballantyne, G.R., Powell, M.S., 2014. Benchmarking comminution energy consumption for the processing of copper and gold ores. Minerals Engineering 65, 109-114.

Bamber, A.S., 2008. Integrated mining, pre-concentration and waste disposal systems for the increased sustainability of hard rock metal mining, PhD, Faculty of Graduate Studies, Mining Engineering. University of British Columbia, Vancouver, Canada.

Berglund, G., Forssberg, E., 1980. Seletiv uppvarmning med mikrovagor, Minfo Rapport, 0703, Sweden.

BGS, 2007. Copper, Mineral Profiles. British Geological Survey, Minerals UK.

Chen, T., Dutrizac, J., Haque, K., Wyslouzil, W., Kashyap, S., 1984. The relative transparency of minerals to microwave radiation. Canadian Metallurgical Quarterly 23, 349-351.

Chunpeng, L., Yousheng, X., Yixin, H., 1990. Application of microwave radiation to extractive metallurgy. Journal of Materials Science and Technology (China) 6, 121-124.

Church, R.H., Webb, W.E., Salsman, J., 1988. Dielectric properties of low-loss minerals. US Department of the Interior, Volume 9194 of Report of Investigations, US Bureau of Mines.

Daniel, M., Lewis-Gray, E., 2011. Comminution efficiency attracts attention. The AusIMM Bulletin 5, 18-28.

Dimitrakis, G., Kingman, S., Dodds, C., Katrib, J., Batchelor, A.R., Jones, D.A., 2014. Sorting mined material, Patent: WO 2014082135 A1. Technological Resources Pty Ltd, PCT/AU2013/001390, Australia.

Dormenval, T., Harding, D., Wellwood, G., 2014. Sorting mined material, Patent: WO 2014183151 A1. Technological Resources Pty Ltd, PCT/AU2014/000500, Australia.

Drinkwater, D., Napier-Munn, T.J., Ballantyne, G., 2012. Energy reduction through eco-efficient comminution strategies, 26th International Mineral Processing Congress, IMPC 2012: Innovative Processing for Sustainable Growth-Conference Proceedings. Technowrites, pp. 1223-1229.

FEI, 2016. Mineral Liberation Analyser (MLA), http://www.fei.com/products/sem/mla/.

Ghosh, A., Nayak, B., Das, T.K., Palit Sagar, S., 2013. A non-invasive technique for sorting of alumina-rich iron ores. Minerals Engineering 45, 55-58.

Ghosh, A., Sharma, A.K., Nayak, B., Sagar, S.P., 2014. Infrared thermography: An approach for iron ore gradation. Minerals Engineering 62, 85-90.

Harding, D., Wellwood, G., 2010. Sorting mined material, Patent: WO 2010028447 A1. Technological Resources Pty Ltd, PCT/AU2009/001200, Australia.

Harrison, P.C., 1997. A fundamental study of the effects of 2.45GHz microwave radiation on the properties of minerals. The University of Birmingham, Birmingham, UK.

John, R.S., Batchelor, A.R., Ivanov, D., Udoudo, O.B., Jones, D.A., Dodds, C., Kingman, S.W., 2015. Understanding microwave induced sorting of porphyry copper ores. Minerals Engineering 84, 77-87.

Jokovic, V., Rizmanoski, V., Djordjevic, N., Morrison, R., 2014. FDTD simulation of microwave heating of variable feed. Minerals Engineering 59, 12-16.

Katrib, J., Dimitrakis, G., Batchelor, A.R., Dodds, C., Kingman, S.W., 2016. Design of a high throughput continuous microwave system. Computers and Chemical Engineering (Under Review).

Kingman, S.W., Dimitrakis, G., Dodds, C., 2013. Microwave applicator, Patent: WO 2013067574 A1. Technological Resources Pty Ltd, PCT/AU2012/001360, Australia.

Kingman, S.W., Vorster, W., Rowson, N.A., 2000. The influence of mineralogy on microwave assisted grinding. Minerals Engineering 13, 313-327.

Knapp, H., Neubert, K., Schropp, C., Wotruba, H., 2014. Viable Applications of Sensor‐Based Sorting for the Processing of Mineral Resources. ChemBioEng Reviews 1, 86-95.

Kobusheshe, J., 2010. Microwave enhanced processing of ores. University of Nottingham, Nottingham, UK.

Lessard, J., de Bakker, J., McHugh, L., 2014. Development of ore sorting and its impact on mineral processing economics. Minerals Engineering 65, 88-97.

Lessard, J., Sweetser, W., Bartram, K., Figueroa, J., McHugh, L., 2016. Bridging the gap: Understanding the economic impact of ore sorting on a mineral processing circuit. Minerals Engineering 91, 92-99.

McGill, S., Walkiewicz, J., 1987. Applications of microwave energy in extractive metallurgy. Journal of Microwave Power and Electromagnetic Energy 22, 175-177.

McGill, S., Walkiewicz, J., Smyres, G., 1988. The effects of power level on the microwave heating of selected chemicals and minerals, Materials Research Society Proceedings. Cambridge University Press, pp. 247-252.

http://dx.doi.org/10.1016/j.mineng.2016.07.007

Murphy, B., van Zyl, J., Domingo, G., 2012. Underground preconcentration by ore sorting and coarse gravity separation, Narrow Vein Mining Conference, Perth, March, pp. 26-27.

Napier-Munn, T., 2015. Is progress in energy-efficient comminution doomed? Minerals Engineering 73, 1-6.

Nelson, S., Lindroth, D., Blake, R., 1989. Dielectric properties of selected minerals at 1 to 22 GHz. Geophysics 54, 1344-1349.

Pascoe, R.D., Udoudo, O.B., Glass, H.J., 2010. Efficiency of automated sorter performance based on particle proximity information. Minerals Engineering 23, 806-812.

Pokrajcic, Z., Morrison, R., Johnson, B., 2009. Designing for a reduced carbon footprint at Greenfield and operating comminution plants, Recent Advances in Mineral Processing Plant Design. Society for Mining, Metallurgy, and Exploration, pp. 560-570.

Powell, M., Bye, A., 2009. Beyond mine-to-mill: Circuit design for energy efficient resource utilisation, Tenth Mill Operators Conference 2009, Proceedings. AusIMM, pp. 357-364.

Riedel, F., Dehler, M., 2010. Recovery of unliberated diamonds by X-ray transmission sorting, Diamonds-Source to Use. The South African Institute of Mining and Metallurgy.

Rizmanoski, V., Jokovic, V., 2016. Synthetic Ore Samples to Test Microwave/RF Applicators and Processes. Journal of Materials Processing Technology 230, 50-61.

Salter, J.D., Wyatt, N.P.G., 1991. Sorting in the minerals industry: Past, present and future. Minerals Engineering 4, 779-796.

Seerane, K., Rech, G., 2011. Investigation of sorting technology to remove hard pebbles and recover copper bearing rocks from an autogenous milling circuit, 6th Southern African Base Metals Conference. The South African Institute of Mining and Metallurgy, pp. 123-136.

Sivamohan, R., Forssberg, E., 1991. Electronic sorting and other preconcentration methods. Minerals Engineering 4, 797-814.

Standish, N., Worner, H., 1991. Microwave application in the reduction of metal oxides with carbon. Iron & Steelmaker 18, 59-61.

Tucker, J., Morrison, R., Wellwood, G., 2013. The development of indices to assess both the sorting potential of an ore and the performance of any sorting process when treating that ore, Physical Separation '13. Minerals Engineering International, Falmouth, Cornwall, UK, pp. 1-12.

Udoudo, O.B., 2010. Modelling the efficiency of an automated sensor-based sorter, PhD, Earth Resources. The University of Exeter, Exeter, UK.

Van Weert, G., Kondos, P., 2007. Infrared recognition of high sulphide and carbonaceous rocks after microwave heating, 39th Annual Meeting of the Canadian Mineral Processors, Ottowa, Ontario, Canada, pp. 345-363.

Van Weert, G., Kondos, P., Gluck, E., 2009. Upgrading molybdenite ores between mine and mill using microwave/infrared (MW/IR) sorting technology, 41st Annual Meeting of the Canadian Mineral Processors, Ottowa, Ontario, Canada.

Walkiewicz, J., Kazonich, G., McGill, S., 1988. Microwave heating characteristics of selected minerals and compounds. Minerals and Metallurgical Processing 5, 39-42.

Wotruba, H., Scharrenbach, T., 2007. New developments in sorting technology - The use of microwave excitation and infrared sensors for ore sorting, Meddelanden fran MinFo No. 37: Conference in Mineral Processing. Swedish Mineral Processing Research Association, Lulea, Sweden, pp. 212-219.

Yixin, H., Chunpeng, L., 1996. Heating rate of minerals and compounds in microwave field. Transactions of Non-Ferrous Metals Society of China 6, 35-40.

http://dx.doi.org/10.1016/j.mineng.2016.07.007

Supplementary Information

Table S.1

Head assays

Sample ID	Sample Grade	Copper (%)	Iron (%)	Sulphur (%)	Chalcopyrite (Cp) [a] (%)	Pyrite (Py) [b] (%)	Moisture (M) (%)	Cp : Py : M
Mine 1								
-50.8+25.4mm								
1	Ore	0.385	4.084	1.356	1.112	1.817	0.178	0.36 : 0.58 : 0.06
2	Ore	2.091	5.305	4.059	6.039	3.705	0.140	0.61 : 0.37 : 0.01
3	Ore	0.964	3.943	1.335	2.785	0.740	0.348	0.72 : 0.19 : 0.09
4	Ore	0.653	4.868	3.615	1.885	5.539	0.271	0.24 : 0.72 : 0.04
5	Ore	0.559	4.191	1.511	1.615	1.775	0.206	0.45 : 0.49 : 0.06
6	Ore	0.954	4.120	1.601	2.755	1.250	0.418	0.62 : 0.28 : 0.09
7	Ore	0.733	3.449	1.839	2.117	2.072	0.137	0.49 : 0.48 : 0.03
8	Waste	0.046	6.486	0.422	0.133	0.707	0.164	0.13 : 0.70 : 0.16
Mine 2								
-50.8+25.4mm								
9	Ore	0.415	4.527	2.312	1.199	3.544	0.874	0.21 : 0.63 : 0.16
9W	Waste	0.120	3.845	1.990	0.345	3.498	0.468	0.08 : 0.81 : 0.11
10	Ore	0.707	1.344	1.061	2.043	0.698	0.193	0.70 : 0.24 : 0.07
10W	Waste	0.255	1.350	1.271	0.737	1.897	0.257	0.25 : 0.66 : 0.09
11	Ore	0.265	9.205	5.202	0.766	9.236	0.611	0.07 : 0.87 : 0.06
11W	Waste	0.260	4.560	2.632	0.750	4.438	0.391	0.13 : 0.80 : 0.07
12	Ore	0.365	3.844	1.105	1.055	1.404	0.614	0.34 : 0.46 : 0.20
13	Ore	0.252	2.683	1.418	0.727	2.264	0.713	0.20 : 0.61 : 0.19
-76.2+50.8mm								
9	Ore	0.287	4.414	2.836	0.830	4.767	0.703	0.13 : 0.76 : 0.11
9W	Waste	0.140	5.409	2.428	0.405	4.278	0.594	0.08 : 0.81 : 0.11
10	Ore	0.753	1.265	0.921	2.174	0.365	0.132	0.81 : 0.14 : 0.05
10W	Waste	0.202	1.423	1.209	0.583	1.880	0.163	0.22 : 0.72 : 0.06
11	Ore	0.210	9.524	5.188	0.607	9.312	0.309	0.06 : 0.91 : 0.03
11W	Waste	0.259	5.146	3.858	0.747	6.735	0.372	0.10 : 0.86 : 0.05
-25.4+12.7mm								
9	Ore	0.571	4.960	2.193	1.650	3.029	0.588	0.31 : 0.58 : 0.11
9W	Waste	0.163	4.672	3.215	0.472	5.708	0.650	0.07 : 0.84 : 0.10
10	Ore	0.656	1.267	0.909	1.894	0.484	0.232	0.73 : 0.19 : 0.09
10W	Waste	0.273	1.529	1.396	0.788	2.097	0.082	0.27 : 0.71 : 0.03
11	Ore	0.342	10.498	5.965	0.987	10.515	0.571	0.08 : 0.87 : 0.05
11W	Waste	0.293	4.583	2.612	0.848	4.337	0.330	0.15 : 0.79 : 0.06

[a] Chalcopyrite assumed to be the only copper sulphide mineral and calculated stoichiometrically from copper content.
[b] Pyrite includes minor molybdenite, which are assumed to be the only other sulphide minerals present and calculated stoichiometrically from molybdenum content and the sulphur balance on copper and molybdenum sulphides.

http://dx.doi.org/10.1016/j.mineng.2016.07.007

Table S.2

Mass and copper distributions across copper grade classes

Sample ID	Sample Grade	Mass Distribution (%)					Copper Distribution (%)				
		Barren	Marginal Grade	Low Grade	High Grade	Very High Grade	Barren	Marginal Grade	Low Grade	High Grade	Very High Grade
		<0.1%Cu	0.1-0.25%Cu	0.25-0.5%Cu	0.5-1%Cu	>1%Cu	<0.1%Cu	0.1-0.25%Cu	0.25-0.5%Cu	0.5-1%Cu	>1%Cu
Mine 1											
-50.8+25.4mm											
1	Ore	26.1	38.6	19.0	5.4	10.9	3.4	15.7	17.2	9.8	53.8
2	Ore	0.0	0.5	4.4	24.5	70.6	0.0	0.0	0.8	9.2	90.0
3	Ore	4.7	11.0	13.6	30.2	40.5	0.3	2.0	5.2	23.5	69.0
4	Ore	20.4	26.0	15.5	20.8	17.4	1.9	6.7	8.0	21.8	61.5
5	Ore	13.6	21.5	22.2	27.6	15.1	1.5	6.9	14.9	35.2	41.5
6	Ore	5.0	5.5	19.7	31.1	38.7	0.4	0.9	7.7	23.1	67.9
7	Ore	6.1	14.7	14.1	37.5	27.6	0.5	3.6	7.3	34.5	54.2
8	Waste	91.6	7.9	0.0	0.5	0.0	67.4	26.8	0.0	5.8	0.0
Mine 2											
-50.8+25.4mm											
9	Ore	9.0	29.2	36.4	18.8	6.6	0.8	12.6	33.0	34.3	19.4
9W	Waste	41.2	48.9	9.9	0.0	0.0	14.6	61.8	23.5	0.0	0.0
10	Ore	0.0	2.1	43.0	35.1	19.8	0.0	0.6	23.3	34.8	41.2
10W	Waste	25.2	44.4	16.4	14.0	0.0	5.5	29.3	23.1	42.0	0.0
11	Ore	36.7	31.4	18.7	11.4	1.8	7.5	20.7	24.6	31.0	16.2
11W	Waste	37.5	30.5	22.1	4.9	5.0	5.6	19.6	30.1	11.9	32.9
12	Ore	28.4	16.6	31.6	16.4	7.0	2.6	9.2	30.6	31.9	25.7
13	Ore	39.1	41.7	10.6	2.7	5.9	6.7	25.9	14.5	6.1	46.9
-76.2+50.8mm											
9	Ore	14.8	45.3	18.1	18.7	3.1	3.1	25.1	19.8	40.9	11.1
9W	Waste	37.6	52.8	9.6	0.0	0.0	16.8	55.7	27.5	0.0	0.0
10	Ore	0.0	2.5	30.1	42.5	24.8	0.0	0.7	16.1	39.1	44.1
10W	Waste	35.2	38.3	18.5	8.0	0.0	6.9	28.5	38.3	26.3	0.0
11	Ore	24.9	46.5	22.1	6.6	0.0	6.4	35.2	36.2	22.2	0.0
11W	Waste	35.6	30.2	17.7	13.2	3.3	5.5	19.7	22.7	32.5	19.5
-25.4+12.7mm											
9	Ore	15.7	14.7	28.4	22.2	18.9	1.2	4.1	18.5	25.8	50.3
9W	Waste	59.2	27.8	4.3	4.0	4.8	14.0	27.0	8.0	16.7	34.3
10	Ore	1.0	8.0	36.4	34.9	19.8	0.1	2.3	20.3	35.6	41.7
10W	Waste	38.9	39.8	9.2	7.8	4.4	6.6	24.6	10.5	20.4	37.9
11	Ore	45.8	10.7	18.9	14.2	10.3	5.0	5.2	17.7	29.3	42.8
11W	Waste	39.1	30.1	15.8	6.7	8.2	6.8	17.2	19.9	15.3	40.9

http://dx.doi.org/10.1016/j.mineng.2016.07.007

Table S.3

Sortability performance indices (O1)

Sample ID	Sample Grade	Intrinsic Sortability Factor, I_{XX}			Sortability Performance Index, P_{XX}		
		I_{25}	I_{50}	I_{75}	P_{25}	P_{50}	P_{75}
Mine 1							
-50.8+25.4mm							
1	Ore	2.92	1.77	1.30	83.4	82.7	76.0
2	Ore	2.28	1.56	1.22	60.4	95.1	90.2
3	Ore	2.03	1.55	1.25	59.7	70.8	55.0
4	Ore	2.84	1.80	1.29	64.5	69.1	80.5
5	Ore	2.27	1.64	1.28	52.1	54.9	67.2
6	Ore	2.03	1.56	1.24	70.5	60.4	51.3
7	Ore	2.02	1.56	1.26	51.9	68.5	82.5
8	Waste	2.45	1.74	1.30	47.1	38.6	49.5
Mine 2							
-50.8+25.4mm							
9	Ore	2.12	1.58	1.24	60.7	44.4	34.7
9W	Waste	1.96	1.53	1.26	3.5	-3.1	41.9
10	Ore	1.94	1.44	1.18	48.9	58.6	46.1
10W	Waste	2.34	1.62	1.27	48.0	56.0	57.4
11	Ore	2.59	1.71	1.26	84.0	64.6	50.0
11W	Waste	2.68	1.77	1.30	32.6	5.0	15.2
12	Ore	2.40	1.69	1.32	-29.2	-1.6	19.8
13	Ore	2.88	1.76	1.30	2.3	14.1	44.0
-76.2+50.8mm							
9	Ore	2.265	1.585	1.233	-14.6	-20.2	10.4
9W	Waste	2.021	1.479	1.221	25.2	34.3	29.0
10	Ore	1.776	1.405	1.175	68.7	51.8	44.7
10W	Waste	2.495	1.678	1.302	38.7	55.5	42.6
11	Ore	2.124	1.567	1.248	16.1	69.7	65.4
11W	Waste	2.575	1.737	1.297	51.2	38.2	19.5
-25.4+12.7mm							
9	Ore	2.368	1.662	1.287	28.6	25.7	22.6
9W	Waste	2.945	1.804	1.319	38.5	49.6	48.1
10	Ore	1.953	1.470	1.203	53.3	70.1	49.6
10W	Waste	2.905	1.755	1.286	72.5	67.5	74.4
11	Ore	2.933	1.848	1.319	66.1	67.9	74.3
11W	Waste	2.819	1.771	1.304	32.1	16.4	-20.2

http://dx.doi.org/10.1016/j.mineng.2016.07.007